# Simultaneous ex-situ CO 2 mineral sequestration and hydrogen production from olivine-bearing mine tailings

Kanchana Kularatne, Olivier Sissmann, Eric Kohler, Michel Chardin, Sonia Noirez, Isabelle Martinez

**HAL Id: hal-01894631**
**https://ifp.hal.science/hal-01894631**

Submitted on 18 Oct 2018

1 **Simultaneous ex-situ CO$_2$ mineral sequestration and hydrogen production**

2 **from olivine-bearing mine tailings**

3

4 [a,b] [*]**Kanchana Kularatne**

5 *corresponding author

6 [a]IFP Energies Nouvelles, 1- 4 Avenue du Bois Préau, 92852 Rueil-Malmaison, France

7 [b]Institut de Physique du Globe de Paris, Sorbonne Paris Cité, Université Paris Diderot, UMR
8 7154 CNRS, 1 rue Jussieu, F-75005 Paris, France

9 e mail : kularatne@ipgp.fr

10 Present address: Institut de Physique du Globe de Paris, 1 rue Jussieu, F-75005 Paris, France

11

12 [a]**Olivier Sissmann**

13 [a]IFP Energies Nouvelles, 1- 4 Avenue du Bois Préau, 92852 Rueil-Malmaison, France

14 e mail : olivier.sissmann@ifpen.fr

15

16 [a]**Eric Kohler**

17 [a]IFP Energies Nouvelles, 1- 4 Avenue du Bois Préau, 92852 Rueil-Malmaison, France

18 e mail : eric.kohler@ifpen.fr

19

20 [a]**Michel Chardin**

21 [a]IFP Energies Nouvelles, 1- 4 Avenue du Bois Préau, 92852 Rueil-Malmaison, France

22 e mail : michel.chardin@ifp.fr

23

24 [a]**Sonia Noirez**

25 [a]IFP Energies Nouvelles, 1- 4 Avenue du Bois Préau, 92852 Rueil-Malmaison, France

26 e mail : sonia.noirez@ifp.fr

27

28    **ᵇIsabelle Martinez**

29    ᵇInstitut de Physique du Globe de Paris, Sorbonne Paris Cité, Université Paris Diderot, UMR
30    7154 CNRS, 1 rue Jussieu, F-75005 Paris, France

31    e mail : martinez@ipgp.fr

32

33    **Abstract**

34    Hydrothermal alteration batch experiments were conducted on olivine bearing mine tailings in

35    order to investigate two potential valorization methods: the ex-situ $CO_2$ sequestration and

36    hydrogen production. The originality of this work lies in the simultaneous investigation of these

37    two processes. We reacted powdered mine tailings with $CO_2$-saturated water at three different

38    sets of P/T conditions, 473K/ 15 MPa, 523 K/30 MPa and 573K/30 MPa. After 25 days of

39    reaction, $CO_2$ was sequestered in the form of Fe-bearing magnesite, $(Mg,Fe)CO_3$ in all the

40    experiments. Maximum carbonation yield was achieved at 523 K and 30 MPa, which was 53.8

41    wt.% of product, equivalent to the trapping of 320.5 g of $CO_2$ per kg of mine tailings. Hydrogen

42    gas was produced via the oxidation of $Fe^{2+}$ in olivine. The highest quantity of hydrogen ($H_2$)

43    was produced at 573 K/ 30 MPa which was 0.57 g of $H_2$ per kg of mine tailings. It suggests that

44    the temperatures between 523 K and 540 K at $pCO_2=30$ MPa are favorable for simultaneous ex-

45    situ $CO_2$ mineral sequestration and hydrogen production from New Caledonian mine tailings.

46        The combined method of ex-situ $CO_2$ storage and hydrogen production proposed by

47    this study offsets 90% of New Caledonia's annual $CO_2$ emissions while compensating ~10 % of

48    New Caledonia's annual energy demand. More globally, it has implications for cost effective

49    disposal of industrial $CO_2$ emissions and production of hydrogen gas (clean energy) at a large

50    scale; those two processes could be combined using the residual heat provided by a third one

51    such as the high temperature smelting of ore.

52    Key words: New Caledonia, Nickel, Carbonation, Hydrogen, Hydrothermal, Olivine, Glass

## 1. Introduction

Since the industrial revolution, the atmospheric carbon dioxide ($CO_2$) level has been substantially increased up to its present day value of ~407 ppm (NOAA, 2016), eventually causing enormous climatic changes such as global warming, ocean acidification, and glacial melting (Manabe and Stouffer, 1993, Kondo et al., 2018; Zhang et al., 2017; Caecer et al., 2018; Marzeion et al., 2018). Up to 65% of the global $CO_2$ emissions were attributed to fossil fuel combustion (Edenhofer et al., 2014), directing the $CO_2$ mitigation measures essentially towards $CO_2$ sequestration mechanisms and introduction of alternate energy sources to fossil fuels.

Scientists have considered the $CO_2$ sequestration in minerals as the so-called permanent method to capture and store industrial emissions of $CO_2$. This method was first suggested by Seifritz (1990), based on the natural phenomena of silicate weathering into carbonates (Abu-Jaber and Kimberley, 1992; Ece et al., 2005; Lugli et al., 2000; Oskierski et al., 2013; Palinkaš et al., 2012; Zedef et al., 2000), during which $CO_2$ reacts with silicates precipitating thermodynamically stable solid carbonates as given by the generalized equation below:

$$M_xSi_yO_{(x+2y-n)}(OH)_{2n} + xCO_2 = xMCO_3 + ySiO_2 + nH_2O \qquad \text{(Eq. 1)}$$
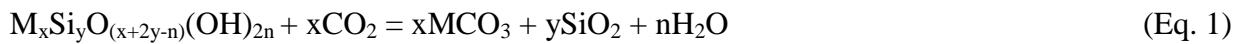
where ($M^{2+}$) represents a divalent cation such as, $Fe^{2+}$, $Mg^{2+}$ and $Ca^{2+}$ in a silicate mineral, and $MCO_3$ thus represents the carbonate incorporating the element M. Once $CO_2$ is converted into a carbonate following reaction (1), it will not be released into the atmosphere over geological time scales.

For the last three decades various aspects of $CO_2$ mineral sequestration have been experimentally investigated, on several mafic minerals such as olivine, serpentine, and pyroxenes (Johnson et al., 2014; Béarat et al., 2006; King et al., 2010; Sissmann et al., 2013; Daval et al., 2009a; Wolff-Boenisch et al., 2006., Park et al., 2003). Among the minerals which consist of divalent Ca, Mg or Fe in their structure, olivine (($Mg,Fe)_2SiO_4$) is considered the most

3

77 favorable for carbonation due to several reasons. Firstly, olivine is abundant in nature in mafic

78 and ultramafic environments (e.g. basalt, peridotites, and dunites). Secondly, it's one of the

79 fastest dissolving silicates (Guthrie, 2001; Brantley, 2003; Golubev et al., 2005; Wolff-Boenisch

80 et al., 2006). Olivine, which contains both Fe and Mg, may form Fe-bearing magnesite

81 ($(Mg,Fe)CO_3$) during the carbonation process, according to equation (2):

82 $(Mg,Fe)_2SiO_{4(s)} + 2CO_{2(aq)} \rightarrow 2(Mg,Fe)CO_{3(s)} + SiO_{2(aq)}$ (Eq. 2)
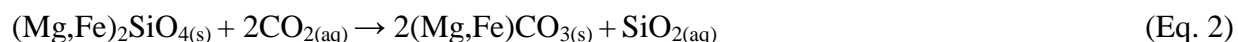
83       Gerdemann et al. (2007), who conducted carbonation experiments on olivine under a

84 wide range of temperature (298 K < T < 523 K) and $CO_2$ partial pressure (1 MPa< $pCO_2$ < 25

85 MPa), have shown that olivine (<75 μm) could be carbonated efficiently, with ca. 85%

86 completion of reaction within an extremely short period of time (around 6 hours), by reacting

87 with a solution of 0.64M $NaHCO_3$ + 1M NaCl, at T = 458 K and $pCO_2$ = 15 MPa. This study

88 also demonstrated that the extent of olivine carbonation is directly proportional to the $CO_2$

89 partial pressure in the system ($pCO_2$). In addition, the authors showed that, at a given $pCO_2$, the

90 extent of carbonation was negligible at lower temperatures (<363 K), while a decrease in the

91 extent of reaction was observed at high temperatures (>458 K). It indicated that at low

92 temperatures, the carbonation reaction is kinetically not favorable due to slow mineral

93 dissolution, whereas if the temperature is too high, although mineral dissolution is kinetically

94 favorable, the extent of carbonation nevertheless decreases. This is due to the formation of Mg-

95 rich phyllosilicates during the competing reaction of serpentinization, in which extensive

96 oxidation of $Fe^{2+}$ also occurs, producing hydrogen, as shown by:

97 $(Mg,Fe)_2SiO_4 + nH_2O \rightarrow x(Mg,Fe^{2+}, Fe^{3+})_3(Si,Fe^{3+})_2O_5(OH)_4 + y(Mg,Fe)(OH)_2 + zFe_3O_4 + (n-2x-y) H_2$ (Eq. 3)

98   (olivine)         (serpentine)       (brucite)    (magnetite)
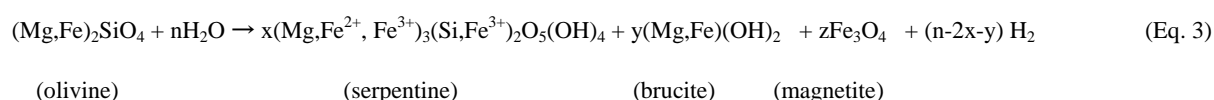
99       The stoichiometric parameters n, x, y and z in this equation strongly depend on how

100 iron is partitioned among the reaction products (McCollom et al., 2016). Large quantities of

101 hydrogen are added to the deep sea floor by this reaction which takes place at the mid oceanic

102 ridge hydrothermal systems.  A number of studies reported the temperature, thermodynamic, and

103 compositional controls on serpentinization (Janecky and Seyfried, 1986; Klein et al., 2013,

104 2009; Klein and Garrido, 2010; McCollom et al., 2016; McCollom and Bach, 2009a; Seyfried et

105 al., 2007). Two important information from these studies indicate that high temperatures (~573

106 K) favor large quantities of hydrogen due to (i) an increase of overall reaction rate of

107 serpentinization, and (ii) an increased partitioning of Fe into brucite ($Mg(OH)_2$), rather than  into

108 magnetite ($Fe_3O_4$). In addition to the hydrothermal alteration of olivine, pure iron or iron-rich

109 materials have also been experimentally studied for hydrogen production (Crouzet et al., 2017;

110 Malvoisin et al., 2013).

111 Olivine, which contains both Mg and Fe, could therefore be favorable for simultaneous

112 $CO_2$ mineral sequestration and hydrogen production, when reacting within a specific range of

113 pressure, temperature and pH conditions, under which carbonation and serpentinization

114 reactions will not inhibit one another. Therefore, this method is a clear improvement on current

115 $CO_2$ mitigation methods, as it proposes reduction of $CO_2$ emissions by mineral storage, and also

116 hydrogen production which is a green energy source. Compared to Fe-Mg-bearing pure minerals

117 or rocks, mine tailings serve as an alternative source of mineral alkalinity that are readily and

118 cheaply available (Bobicki et al., 2012), and can be valorized by the above method (Bobicki et

119 al., 2012; Harrison et al., 2016, 2013; Power et al., 2013; Wilson et al., 2014; Malvoisin et al,

120 2013). However, these previous studies on mine tailings have only focused on either $CO_2$

121 storage or $H_2$ production separately. The present study aims to investigate the potential of

122 combining the strategy of $CO_2$ mineral storage with hydrogen production by reacting olivine-

123 bearing mine waste material obtained from nickel (Ni) extraction mines in New Caledonia. In

124 order to maintain both of these reactions, the mine tailings were reacted with $CO_2$-saturated

125 water at P/T range slightly inferior to the conditions previously identified as optimum for ex-situ

126 carbonation (Gerdemann et al., 2007), and close to optimum hydrogen production in

127 hydrothermal systems (McCollom et al., 2016; McCollom and Bach, 2009a; McCollom and

128 Bach, 2008; Tutolo et al., 2018; Meyhew et al., 2018). We present the quantities of $CO_2$ that can

129 be stored in mine tailings, and the quantities of $H_2$ that can be produced by this method. Based

130 on these experimental values, we estimated the $CO_2$ offset and compensation of energy demand

131 of New Caledonia. Although the application of this process is centered on New Caledonian mine

132 tailings, it could be translated to other industrial sites where Mg and Fe remain major

133 components of the wastes after ore processing.

134 **2. Materials and methods**

135 **2.1 Starting materials**

136 All the experiments were performed on olivine bearing mine tailings from industrial

137 nickel (Ni) extraction sites in New Caledonia, where Ni is extracted from laterite and saprolite

138 ores (Wacaster, 2013). The hand specimens of mine tailings consisted of light- to dark-green

139 irregular shaped grains with sizes ranging from few millimeters to < 1 cm. The X-ray diffraction

140 (XRD) analysis performed on a finely powdered sample indicated the presence of olivine, traces

141 of enstatite and an amorphous phase (glass). The amount of glass was quantified by XRD

142 Rietveld analysis performed on the diffraction pattern of a mixture of powdered mine tailings

143 and alumina (20 wt.%) where alumina serves as the internal standard (Bish and Howard, 1988;

144 Bish and Post, 1993; McCusker et al., 1999). According to this analysis the sample was

145 composed of 55 wt.% of glass and 45 wt.% of crystalline olivine. The chemical composition of

146 mine tailings was obtained by electron probe micro analysis (EPMA) operated at 15 keV and 40

147 nA, on few randomly selected macroscopic grains mounted on epoxy resin. The analysis was

148 performed on multiple points on glass and olivine, which appeared texturally different under

149 SEM, and the average compositions were reported in Table 1. This is in good agreement with

150     the composition reported by Bodénan et al. (2014), who used the same material for $CO_2$

151     sequestration experiments. The magnesium numbers (Mg#=Mg/(Mg+Fe)) of the glass and

152     crystalline olivine were 0.75 and 0.88 respectively, and were calculated on molar basis using the

153     average oxide wt.%.

154           Mine tailings were crushed in a ball mill to obtain 40 - 63 μm size fraction. This size

155     fraction was chosen in order to maintain rapid dissolution kinetics, as well as to facilitate

156     microscopic observations. Furthermore, those grain sizes are in the same range than those used

157     in the few previous studies on hydrogen generation (Malvoisin et al., 2013, 2012a, 2012b), thus

158     making the comparison easier. Even though the choice of nano-scale particles could have

159     provided a considerably faster reaction, the mineral surfaces available for microscopic studies of

160     the products would have been limited. Finally, for industrial purposes, grinding large quantities

161     of solid down to the nanometer scale would largely increase the cost of the process.

162           The selected sieve fraction was subsequently ultrasonically cleaned in ethanol for 8-

163     10 min to remove the fine particles adhered to the surface. This process was repeated until the

164     supernatant became clear. The powder was dried in oven at 343 K overnight after cleaning with

165     ultra-pure de-ionized water (electrical conductivity = 18.2 MΩ cm). Very few fine particles

166     remained adhering to the grain surfaces of the above dried powder, when observed under SEM

167     (Figure 1a). The specific surface area (SSA) of the cleaned starting powder was determined by

168     Kr adsorption analysis, according to the Brunauer–Emmett–Teller (BET) method (Brunauer et

169     al., 1938), yielding a value of 0.23 $m^2$/g.

170           Scanning electron microscopic (SEM) analysis performed on a polished section of

171     mine tailings indicate that it consists of inclusion of free and textured glass with embedded

172     olivine crystals, resulting in a "dendritic texture" or a "quench texture" (Figure 1b). The glass

173     and dendritic texture were assumed to be the result of two steps in the ore processing. The first

174     is the "calcination" performed by pre heating the ore at >1173 K for moisture removal and first

7

175     phase of metal oxide reduction. The second is the "fusion reduction" by which the ore is melted

176     using an electrode operated at <1973 K, separating Ni from the residue or mine tailings. We

177     assume that these conditions reached the "dry" melting-point of peridotite (-approximate

178     composition for the ophiolite) under atmospheric pressure (Takahashi, 1986), where olivine can

179     coexist with pyroxene melt up to about 2023 K at 1 atm during the eutectic melting of peridotite,

180     which could probably explain the quench texture in mine tailings.

181     **2.2 High pressure and high temperature experiments**

182     Three batch experiments were conducted at different P/T conditions, in order to

183     investigate the most favorable conditions for simultaneous $CO_2$ sequestration and $H_2$ production.

184     All the experiments were performed in 250 ml volume Parr[®] hastelloy stirring- type batch

185     reactors (impeller speed, 100 r.p.m), with a $TiO_2$ inner lining. Powdered mine tailings and

186     deionized water (1:100 mass ratio) were added to the batch reactors and pressurized with $CO_2$

187     (99.9% purity).

188     The first experiment (MT1) was conducted at 473K/ 15 MPa, which was slightly

189     above the known optimum temperature reported for the $CO_2$ mineral sequestration, i.e. 453 K/15

190     MPa, using a solution of 0.64M $NaHCO_3$/1M NaCl. The second and third experiments were

191     conducted at P/T conditions more favorable for $H_2$ production by serpentinization, such as 473

192     K and 673 K and 30-50 MPa (Allen and Seyfried, 2003; Andreani et al., 2012; Berndt et al.,

193     1996; Janecky and Seyfried, 1986; Malvoisin et al., 2012a; McCollom and Bach, 2009b;

194     McCollom and Seewald, 2001). These conditions are known to accelerate the serpentinization

195     rate while producing large amounts of $H_2$. The second experiment (MT2) was thus conducted at

196     523 K/30 MPa, both temperature and pressure being slightly above MT1. The third experiment

197     (MT4) was performed at 573 K/30 MPa. Two more experiments were conducted as blank runs

198     (MT2b, and MT4b) to determine possible contaminations in gas phase. They were conducted

199     under similar conditions (-in terms of amount of water, $pCO_2$, T) to those of MT2 and MT4, but

200   without any solid phases added in the reactor. Details of these experiments are reported in Table

201   2. The run duration of all the experiments was approximately 25 days. The $pCO_2$ of the

202   experiments drops intermittently (0.1 to 0.5 MPa) during the run due to; (i) $CO_2$ consumption by

203   carbonation reaction, and (ii) sampling out aliquots of gas from the batch reactor. The pressure

204   was re-adjusted to the initial pressure by pumping $CO_2$ gas back to the batch reactor. At the end

205   of the 25-days run, the experiments were quenched rapidly to ambient conditions by cooling the

206   reactor cell in a water bath for ~20-30 min. The autoclaves were then opened right after

207   releasing the pressurized $CO_2$ inside the reactor, minimizing the potential formation of secondary

208   products at this stage. The solid products were recovered and oven-dried at 333 K overnight,

209   then used for further analysis, as described below.

210           At these P/T conditions, most of the $CO_2$ pumped into the reactor exists as $CO_{2(aq)}$

211   with a smaller amount of $HCO_{3\ (aq)}^{-}$ and traces of $CO_{3\ (aq)}^{-2}$, which can therefore be summed up to

212   a binary mixture of $CO_2$-$H_2O$ that has not reached critical condition. The initial pH at P/T

213   relevant to experimental conditions was calculated by the CHESS geochemical code  (van der

214   Lee and De Windt, 2002) for each reaction temperature, creating a closed system with water and

215   $CO_2$ ($f$CO_2$ at each P/T conditions was calculated using the Thermosolver program (Barnes and

216   Koretsky, 2004). The experimental conditions and the calculated initial pH of the solutions are

217   reported in Table 2.

**2.3 Sampling and analytical methods**

**2.3.1 Gas sampling and analysis**

220        The gas phase in the head space of the batch reactor was sampled every 2-3 days

221  during the reaction, by connecting a gas-sampling tube to the batch reactor. Before sampling, a

222  vacuum of $10^{-5}$ bars was created along the tubings of the batch reactor and also in the sampling

223  tube. The vacuum was held for about 10-15 min. This procedure ensures the absence of any leak

224  and contaminations in the tubings. Collected gas samples were then analyzed with a Varian CP-

225  3800 gas chromatograph (GC) to identify and quantify the gaseous products of the reaction. For

226  this purpose, two standards were first analyzed: one with an atmospheric composition, and the

227  other being a mixture of $H_2$, He, $N_2$, $CO_2$ and alkanes up to four carbons ($C_1$-$C_4$). The samples

228  and the standards were injected to the GC at ~1200 mbar at room temperature. Before analyzing

229  a standard or a sample, a blank measurement was carried out by injecting $N_2$. Finally, the

230  percentages (%) of each gas in the analyzed samples were calculated using the response factors

231  (k) obtained. The uncertainty on $H_2$, $CO_2$, $CH_4$ and other simple alkanes abundances ($C_2$-$C_4$)

232  measured by GC were 5.4%, 1.3%, 0.6% and ~1.2% respectively.

**2.3.2 Solid product analysis**

234        The mineralogical composition of bulk solid products was obtained through XRD

235  analysis performed on finely powdered reaction products, using a X'Pert PRO (PANalytical) x-

236  ray diffractometer with a Cu anode (Cu K$\alpha$ = 1.5418 Å), operated under 45 kV and 40 mA. The

237  detection limit of XRD is ~1%. Rock-Eval 6 analysis was performed for better detection and

238  quantification of carbonate. The quantification limit of Rock-Eval 6 is ~0.02 wt.% C, which

239  corresponds to ~0.15 wt.% $MgCO_3$; this method is one order of magnitude more sensitive than

240  the phase quantification by XRD. More details on sample preparation, instrumentation and

241  analysis of the Rock-Eval 6 technique can be found in Behar et al. (2001) and Lafargue et al.

242    (1998). The analytical details and the calculation of carbonates are reported in supporting

243    information S6. Energy dispersive X-ray analysis in transmission electron microscope (TEM-

244    EDX) was performed on ultra-thin sections prepared by focused ion beam milling (FIB), in

245    order to obtain the composition of magnesite: more details are given in supporting information

246    S10.

247        A separate fraction of the reaction products was mounted on adhesive carbon-taped

248    sample holders, gold (Au) coated and observed under "high vacuum" conventional SEM, EVO

249    MA 10, Carl Zeiss SMT with a tungsten filament operated under 15 kV and 100 mA. A 150 pA

250    beam was applied for secondary electron (SE) imaging to observe the surface topography with a

251    high spatial resolution, while the back scattered electron detector (BSE) was used to obtain

252    images with atomic number contrast. Qualitative chemical analyses were performed by energy

253    dispersive X-ray analysis (EDX), with a probe current at 700 to 750 pA (Oxford). The silicon

254    drift detector is calibrated on cobalt (Co) for quantitative analyzes during 10 s at 10 to 15 kcps

255    with a dead time of about 15 s. In addition, SEM element mapping was performed on the

256    reaction products mounted on epoxy resin, finely polished by ion beam milling.

257    **2.3.3 Fe(III) / Fe(II) analysis**

258        The amounts of $Fe^{2+}$ and total iron in the non-reacted mine tailings, and the three

259    experimental products were analyzed at the Centre de Recherches Pétrographiques et

260    Géochimiques (CRPG), Nancy, France. The samples were boiled in HF / $H_2SO_4$ to release $Fe^{2+}$

261    which was then quantified by volumetric titration with $K_2Cr_2O_3$. Another fraction of the sample

262    was then heated with $LiBO_2$ at 1223 K and acid digested (4 vol.% $HNO_3$) to convert all species

263    of iron (e.g. $Fe^0$ and $Fe^{2+}$) contained in the sample into $Fe_2O_3$ ($Fe^{3+}$). The resulting ferric iron

264    was measured by atomic absorption spectrophotometer (AAS). The amount of $Fe^{3+}$ in the non-

265    reacted mine tailings sample was calculated by subtracting the $Fe^{2+}$ molar amount measured in

266    the FeO analysis from the ($Fe^{2+} + Fe^{3+}$) amount measured in the $Fe_2O_3$ analysis. The value being

267    close to 0 suggests there is little to no oxidized iron in the initial material. The quantities of $H_2$

268    measured by GC at the end of the experiments were compared to the amounts calculated from

269    the loss of $Fe^{2+}$ (through oxidation and simultaneous $H_2$ production) in the products. In order to

270    estimate the amount of $Fe^{3+}$ formed during the experiments, the amount of $Fe^{2+}$ measured in the

271    products were subtracted from the one measured in the initial non-reacted mine tailings; the

272    quantity of $H_2$ produced was then extrapolated from the oxidized iron ($Fe^{3+}$) according to:

273              $2Fe^{2+}_{(aq)} + 2H_2O_{(l)} = 2Fe^{3+}_{(aq)} + 2OH^-_{(aq)} + H_{2(g)}$                 (Eq. 4)
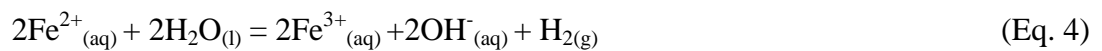
274    where, the stoichiometric proportion of $Fe^{2+}$ : $H_2$ is 2:1.

275    **3.  Results**

276    **3.1 Secondary products**

277    XRD pattern of non-reacted mine tailings and the reaction products of three experiments are

278    shown in Figure 2c. The non-reacted mine tailings sample primarily consisted of olivine. The

279    peaks of corundum (Figure 2c), in this diffraction pattern are due to pure corundum which was

280    added to mine tailings as the internal standard for quantification of glass. The products consisted

281    of Fe-rich magnesite as the major phase, small quantities of phyllosilicates and traces of non-

282    reacted olivine (Figure 2c). Fe-bearing magnesite was identified by the characteristic reflections

283    at $2\theta = 35.9°$ and $50°$ (Giammar et al., 2005; Garcia et al., 2010). SEM element mapping

284    performed on a polished section of MT2 sample showed the presence of abundant magnesite

285    compared to other phases such as olivine, glass, and phyllosilicate, and therefore is well in

286    agreement with the XRD results (Figure 2a). The SEM analysis performed on a carbon-coated

287    reaction product of the same sample indicates the growth of rhombohedral magnesite containing

288    both Fe and Mg, as confirmed by the EDX spectra collected on SEM (Figure 2b). Figure 3

289    shows the SEM analysis performed on polished sections of solid products of the three

290    experiments, each mounted on epoxy resin. At 473 K /15 MPa, mine tailings have been altered,

291    precipitating anhedral magnesite, and thin layers of phyllosilicate (Figure 3a). Magnesites

292    precipitated along a grain of textured mine tailings are shown on Figure 3b. At 523 K /30 MPa,

293    the product contained thick phyllosilicate layers around mine tailings and subhedral magnesite

294    with Fe and Mg compositional zoning (Figure 3c). At 573 K /30 MPa, the products contained

295    anhedral magnesites and mine tailings heavily covered by a thick fibrous phyllosilicate layer

296    (Figure 3c). More SEM images with EDX analysis on these samples are given in supplementary

297    S7, S8 and S9. The chemical composition of magnesites analyzed by TEM-EDX yielded

298    $Mg_{0.92}Fe_{0.08}CO_3$, $Mg_{0.58}Fe_{0.42}CO_3$ and $Mg_{0.83}Fe_{0.17}CO_3$ at 473 K /15 MPa, 523 K /30 MPa and

299    573 K /30 MPa respectively, showing different concentrations of iron further discussed in

300    section 4.2. The details of TEM analysis is given in supplementary information S10.

301    Compared to the diffraction pattern of the non-reacted sample, the peak intensity of

302    olivine gradually decreases with the increasing temperature of the experiments, indicating

303    olivine dissolution has mostly increased along with temperature. The semi-quantitative phase

304    analysis on the collected diffraction patterns indicated that approximately 23.3 wt.%, 9.4 wt.%

305    and 12.2 wt.% of olivine were still remaining in the reaction products of 473 K /15 MPa, 523 K

306    /30 MPa and 573 K /30 MPa experiments respectively. The peaks for phyllosilicates are broad

307    and less intense in all experiments, and the number of phyllosilicate peaks visible on the

308    diffractogram increased with temperature, indicating more phyllosilicates formed with higher

309    temperature. A preliminary identification of these phyllosilicates was obtained by applying a

310    treatment with ethylene glycol to verify their expansion properties, which suggested that they

311    were smectite clay minerals. However, due to the inherent limitations of the equipment, the

312    amount of phyllosilicate and remaining glass could not be quantified separately.

313

314

## 3.2 Carbonate yield

The presence of carbonates and their precise quantification were further confirmed using the Rock-Eval 6 technique. The only carbonate phase produced in all the experiments were Fe-bearing magnesites, $(Mg,Fe)CO_3$, in accordance with the results of XRD analysis. Carbonate quantification by Rock-Eval 6 resulted in 20.3%, 44.9% and 21.6% at 473 K/ 15 MPa, 523 K/ 30 MPa and 573 K/ 30 MPa respectively (the calculation is given in S6); those carbonation yields are averages of duplicate experiments. These yields suggest that 1.00 kg of mine tailings could capture 115g, 321g and 119 g of gaseous $CO_2$ by a reaction with pure water at 473 K/ 15 MPa, 523 K/ 30 MPa and 573 K/ 30 MPa, respectively (Table 2 and S6).

## 3.3 Hydrogen production

As the starting mine tailings material is iron-rich (average of 10.9 wt.%), its reaction with water at high pressure and high temperature leads to the production of $H_2$, as a result of iron oxidation through water reduction (also written for the serpentinization reaction given by eq.3). However, the produced hydrogen in all the experiments is approximately three orders of magnitude lower than the $CO_2$ in the gas phase, since $CO_2$ was injected to reach a total pressure of either 15 or 30 MPa. The variations in gas phase composition in each experiment are given below.

**At 473 K and 15 MPa:** Figure 4a, illustrates the cumulative production of hydrogen as a function of time for MT1. Hydrogen was produced gradually reaching a maximum of 20.0 µmol/g of mine tailings after 25 days of reaction, which indicates that the reaction is still in progress. The maximum hydrogen production of 20.0 µmol/g is equivalent to producing around 0.04 g of $H_2$ for 1.0 kg of mine tailings. Hydrogen was produced at a rate of approximately 0.7 µmol/g/day, obtained by the gradient fitted though the data. Traces of methane (<0.30 µmol/g)

338 were detected in the gas phase after 9.8 days of reaction, but other light hydrocarbons ($C_2$-$C_4$)

339 were not detected (S 1).

340 **<u>At 523 K and 30 MPa:</u>** The cumulative hydrogen production as a function of reaction time of

341 MT2 experiment is shown in Figure 4b. Hydrogen continues to be produced at a rate of 1

342 µmol/g/day until ~9 days, as the reaction proceeds. After 9 days, hydrogen production increases

343 abruptly and then continues to increase at a rate of 3.2 µmol/g/day. The maximum amount of

344 gaseous hydrogen measured in this experiment was 117.6 µmol/g or 0.24 g/kg of mine tailings,

345 which is approximately 5 times more than in MT1. No hydrogen was detected in the gas phase

346 of an experimental blank (MT2b) conducted under the same without adding mine tailings

347 confirming that hydrogen was produced only by reaction between pure water and mine tailings

348 (Figure 4b). Light hydrocarbons such as $CH_4$, $C_2H_6$, $C_3H_8$ and $C_4H_{10}$ were also observed in the

349 gas phases of both the experiment and experimental blank, but in trace quantities (S2 and S4).

350 **<u>At 573 K and 30 MPa:</u>** Cumulative hydrogen production of MT4 experiment is shown in

351 Figure 4c. At the initial stage, hydrogen was produced at a rate of 21 µmol/g/day (0<t<8.8 days),

352 reaching a maximum of 283.5 µmol/g or 0.57 g/kg. This is the highest quantity of hydrogen

353 produced among all three experiments, and is confirmed by the $H_2$ production inferred from iron

354 (III) measured at the end of the experiments (265 µmol/g, see Table 2). Then, the amount of

355 hydrogen decreased drastically, reaching a plateau with an average of 41 µmol/g (Figure 4c).

356 Similarly to MT2, hydrogen was not detected in the gas phase of an experimental blank (MT4b)

357 conducted at the same P/T conditions, which confirmed there was no contamination of hydrogen

358 in the experiment (Figure 4c and S3). This decrease in cumulative hydrogen could be explained

359 by the formation of short-chained organic molecules through its interaction with $CO_2$, as

360 discussed by Seewald (2006). In addition, $CH_4$, $C_2H_6$, $C_3H_8$ and $C_4H_{10}$ were detected in the gas

361 phase, in which the detected methane was above the 10% uncertainty of the concentration

362 detected in the experimental blank (S5).

**3.4 $H_2$ production estimated by Fe(III)/Fe(II) analysis**

As previously stated, hydrogen is produced via the oxidation of $Fe^{2+}$ in the starting material according to equation 4 (section 2.3.4). Therefore, the difference between the amounts of FeO measured in the starting material and the reaction products quantifies the $Fe^{2+}$ that has been oxidized at high pressure and high temperature.

The analysis shows that the starting mine tailings sample contained, 1.3 mmol/g of FeO, whereas the reaction products of MT1, MT2 and MT4 experiments contained 1.3, 1.1 and 0.8 mmol/g of FeO, respectively. According to this result, the initial mine tailings and the MT1 experiment contained the same amount of FeO, meaning that no $Fe^{2+}$ oxidation took place. However, 20 µmol/g of hydrogen was detected in the gas chromatography analysis of this experiment. This could possibly suggest an analytical error in detecting such a low level of FeO quantity due to the detection limit of the method used. The $H_2$ production estimated from the stoichiometric ratio with $Fe^{3+}$ (given in eq. 4) are reported in Table 3 for the three experimental runs. Except for MT1, the estimated values of hydrogen are in good agreement with those observed in gas chromatography analysis.

Moreover, if all the $Fe^{2+}$ in initial mine tailings (i.e. 1.3 mmol/g) was to completely oxidize into $Fe^{3+}$, then following the equation 4 (1 mole of $H_2$ produced for 2 moles of $Fe^{2+}$ oxidized), it could produce 655 µmol of $H_2$ per one gram of mine tailings. This value can be used to calculate the reaction progress with respect to Fe oxidation in the system. Although the value for MT1, as mentioned earlier, is too low and thus unreliable to be properly exploited, the estimation shows that MT2 and MT4 reach 17.6 % and 40.5% completion of reaction respectively (see Table 3).

## 4. Discussion

### 4.1 Preferential dissolution of olivine within mine tailings at 473-573 K and 15-30 MPa

The suitability of geological material as carbon sequestration and hydrogen production feedstocks depends primarily on their reactivity and chemical composition (Power et al., 2013). Mafic and ultramafic rocks are rich in $Ca^{2+}$, $Mg^{2+}$ and $Fe^{2+}$, and therefore, are the ideal sources for this purpose. New Caledonian mine tailings contained abundant $Mg^{2+}$ and $Fe^{2+}$, and thus their chemical composition and reactivity favored $CO_2$ sequestration and hydrogen production. Mineral dissolution, is essentially the first step that makes $Mg^{2+}$ and $Fe^{2+}$ available for both carbonation and hydrogen production reactions, and is a function of crystal chemistry, particle size of reacting mineral, pH, and temperature. As shown in Figure 2, olivine dissolved gradually with increasing temperature of our experiments, indicating that for our grain sizes and pH, increasing temperatures were favoring the dissolution of olivine. Inevitably, XRD pattern does not indicate the dissolution of glass due to its lack of crystallinity. In acidic to neutral pH, the dissolution kinetics of olivine have been reported to be faster than that of basaltic glass, which is an approximation that can be made for mine tailings (Gudbrandsson et al., 2011; Wolff-Boenisch et al., 2006; Wolff-Boenisch et al., 2011). These two previous studies suggest that, under acidic conditions such as those of our study, the constituent minerals of crystalline basalt dissolve faster than basaltic glass by more than one order of magnitude (olivine, a nesosilicate with a $Q_0$ structure, has all silicate tetrahedrons disconnected from each other, as opposed to glass, and thus faster dissolution kinetics). This indicates that olivine is the major contributor to the $Mg^{2+}$ and $Fe^{2+}$ cations in the solution.

### 4.2 Reaction path and formation of secondary Mg-silicates

The XRD patterns of the products indicated that the reaction of mine tailings with $CO_2$-saturated water, resulted in Fe-rich magnesite, and small quantity of phyllosilicates.

409   Hydrogen is the gaseous product of this reaction. Hematite ($Fe_2O_3$) was observed only in MT4

410   (573 K/30 MPa) experiment. Although, we anticipated the production of hydrogen through

411   serpentinization reaction, our result showed that the products of the reaction after 25 days

412   consisted of smectites. However, formation of proto-serpentine-like phase using New

413   Caledonian mine tailings was reported by Bodenan et al. (2014), in an experimental work

414   where 1-day reactions took place either in water or in a 0.43 M NaCl/0.27 M $NaHCO_3$

415   solution at 453 K at a $pCO_2$ of 1-9 MPa.


416         The difference between the reaction products of those two sets of experiments

417   cannot be explained by different pH conditions, as Bodénan et al.(2014) run experiments both

418   in bicarbonate solution (which has the buffer ability to remain neutral under $pCO_2$ pressure),

419   and in deionized water (which becomes acidic). The temperature, though lower in Bodénan et

420   al.'s study (453K), remains close to our study's conditions (473-573K), and grain size (which

421   influences specific surface area) should not have a critical influence on thermodynamic

422   equilibrium. With respect to these parameters, the two studies are comparable, while their

423   reaction products differ. One possible explanation could very well lie in the duration of the

424   experiments. A study investigating the genesis of ultramafic hosted magnesite vein deposits

425   by Abu-Jaber and Kimberly (1992) has reported, within natural samples, on the reaction of

426   serpentine, magnetite and bicarbonate into (Fe-)nontronite (smectite) and magnesite.

427   Furthermore, a recent experimental study describes various pathways for the conversion of

428   serpentine to smectite under hydrothermal conditions, during which $Al^{3+}$ substitutes to $Si^{4+}$.

429   They suggest that solid-state transformation is the main mechanism involved. Since this is a

430   process is kinetically limited, the difference in the experiments duration (1 day for Bodénan et

431   al. vs 25 days for this study) could explain the different reaction product. Serpentine would

432   therefore only be an intermediate phase.


433

**4.3 Fe-rich magnesite precipitation and hydrogen production**

434

435    Fe-rich magnesite was the only carbonate precipitated in our experiments as

436    confirmed by XRD and Rock-Eval 6 analysis. Theoretically, mine tailings could precipitate a

437    maximum of 77 wt.% of magnesite, assuming 100% dissolution of mine tailings (S11). The

438    quantities of Fe-rich magnesite precipitated at 473 K/15 MPa, 523 K/30 MPa and 573 K/30

439    MPa were 20.3, 44.9 and 21.6 wt.%, respectively. If the reaction completion (Rx) with respect

440    to carbonate precipitation is given by the ratio between the observed carbonate wt.% versus

441    the calculated maximum carbonate wt.%, then 26.4%, 58.3% and 28.1% of reaction

442    completion were achieved respectively during the experiments. Interestingly, the iron content

443    in magnesite followed the same trend as reaction completion, with 0.08, 0.58  and 0.17 moles

444    of iron in one mole of magnesite at 473 K/15 MPa, 523 K/30 MPa and 573 K/30 MPa

445    respectively. This would indicate that the lower temperature and low $pCO_2$ in MT1 (473 K/15

446    MPa) slowed down kinetics of the dissolution and precipitation reactions resulting in low

447    quantities of magnesite with small quantity of iron, compared to the other two experiments.

448    The MT2 and MT4 experiments, which were conducted at same $pCO_2$ (30 MPa), revealed that

449    almost all the olivine dissolved at increasing temperature up to 573 K. But, the precipitated

450    magnesite at 523 K was twice higher than at 573 K. As Mg is the major element in magnesite,

451    this result clearly indicates the competition of Mg incorporation into magnesite vs. secondary

452    Mg-silicates in the 523-573 K temperature range. In addition, the quantity of iron

453    incorporated in magnesite at 523 K is twice as high than at 573 K, indicating that

454    temperatures  between 523 -573K favored the incorporation of iron into other phases than

455    magnesite. As shown by Andreani et al. (2012), the fast precipitation of Al-Fe-rich serpentines

456    indeed competes with magnetite nucleation and may indeed inhibit it altogether. Nevertheless,

457    magnetite formation is enhanced with increasing temperature, as shown by Malvoisin et al.,

458    2012); those studies thus support the present observations and findings on Fe(III)

36

459    incorporation into secondary phases. Total iron (II+III) incorporation into secondary phases

460    and its correlation with hydrogen production is also worth mentioning because it demonstrates

461    the competition between two other reactions in the system: the iron incorporation into

462    magnesite versus secondary Mg-silicates (±iron oxides). As the temperature increased from

463    523 K to 573 K, hydrogen production was approximately doubled, producing more $Fe^{3+}$. At

464    523 K, the most likely secondary phase to host $Fe^{3+}$ was secondary phyllosilicate, whereas at

465    573 K, it could possibly be incorporated into phyllosilicate and into iron (III) oxides as well.

466    Although, ferric-hydrate complexes could host $Fe^{3+}$ ions, we assumed their quantities to be

467    negligible. Magnesite structure accommodates only $Fe^{2+}$. Therefore, the results clearly

468    indicate that temperatures between 523 -573K favor iron oxidation, whereas temperatures

469    between 473 K and 523 K favor the iron incorporation into magnesite. The competition

470    between Mg and Fe incorporation among the secondary phases seems to control the quantities

471    of magnesite precipitation and hydrogen production. Moreover, Figure 5, which shows the

472    magnesite production (in wt.%) versus hydrogen production clearly demonstrates that

473    temperatures between 523 K and 540 K at $pCO_2$=30 MPa (shown by shaded area) would be

474    the most favorable conditions for reacting mine tailings in order to maintain both carbonation

475    and hydrogen production in significant quantities. Although the P/T conditions of maximum

476    carbonation in our experiments differ slightly from those of Gerdermann et al. (2007), it can

477    be argued that this discrepancy arises from the different solutions used in two studies; a $CO_2$-

478    saturated water here compared with a 0.64M $NaHCO_3$, 1M NaCl solution in Gerdermann et

479    al. (2007). Furthermore, Andreani et al. (2012) and Sissmann et al. (2013) mention the effect

480    of aluminum on dissolution kinetics of olivine dissolution kinetics. Its presence in the

481    associated glass phase of the mine tailings could also slightly change not only those

482    dissolution kinetics but also the precipitation kinetics of carbonates.

483          The analysis of FeO in the starting material and the products were used to evaluate

484    the amount of iron oxidation, and to further confirm the hydrogen amounts measured by gas

485    chromatography. As mentioned in section 3.4, the Fe(III) / Fe(II) analysis of non-reacted mine

486    tailings confirmed that the starting material does not contain any $Fe^{3+}$ that could have resulted

487    from ore processing. Assuming the mine tailings have been well homogenized after crushing

488    and sieving, the $Fe^{2+}$ measured in the experimental products was expected to be lower than in

489    the initial sample, due to the oxidation of $Fe^{2+}$ during the experiment. However, the amount of

490    $Fe^{2+}$ measured for MT1 is slightly above the value measured for the initial non-reacted

491    sample. Such an inconsistency could be explained by potential inhomogeneities caused by a

492    sampling bias of the starting material or the products, or due to detection limit for low Fe

493    concentrations in this sample. Nevertheless, the estimated hydrogen production from MT2

494    and MT4 experiments are in good agreement with the measured hydrogen quantities using gas

495    chromatography (Table 3).

496          The variation of hydrogen production as a function of reaction time (Figure 4)

497    indicates that the hydrogen production at 473 K/15 MPa and 523 K/ 30 MPa continued to

498    increase steadily until the end of the experiment, whereas at 573 K/30 MPa, it suddenly

499    decreased after 9 days of reaction, reaching a plateau. This result suggests that at the lower

500    temperatures, the production on of $H_2$ is not buffered by new secondary phases (no

501    phyllosilicates passivating the surface of mine tailings). However, at 573K, it appears that

502    hydrogen production is being buffered. A possible explanation would be the limitation of $Fe^{2+}$

503    supply, and thus of further water reduction and $H_2$ production. Nevertheless, the sharp

504    decrease in $H_2$ concentration followed by a plateau could indicate that a steady state has been

505    reached, and that $H_2$ is being consumed to form light organic compounds dissolved within the

506    system (not quantified in this study) through a reaction with $CO_2$.

507

**4.4 Carbonation and hydrogen production from mine tailings vs. other slags**

First our results on $CO_2$ sequestration were compared with two experimental studies by Bobicki et al. (2015) and Garcia et al. (2014), who conducted experiments at T~423 K and $PCO_2$ ~15 MPa. Bobicki et al. (2015) used chrysotile from two nickel (Ni) mines (Okanogan nickel deposit in Washington State, USA (OK ore) and Thompson Nickel Belt in Manitoba, Canada, (Pipe ore), respectively) (table 4). The ores contained 6.0 and 7.8 wt.% of MgO, with approximately <7 wt.% of CaO+FeO. In contrast, Garcia et al. (2010) used pure olivine (Fo91), with 55.5 wt.% of MgO (theoretical), which is also close to the average MgO content of this study (53.6 wt.%), but containing nearly half of the iron compared to mine tailings in this study (12.95 wt.%). Our results on carbonation yields lie within the same order of magnitude compared to the two studies considered here. However, despite the large granulometry of the starting materials, Bobicki et al. (2015) was able to store $CO_2$ at a higher rate (~200 g/kg $CO_2$ within one hour) than the other two studies. They reacted olivine (formed from the reversion of heat-treated chrysotile) at the conditions previously suggested by Gerdemann et al. (2007), making solution salinity and bicarbonate concentration the main differences with the other two studies. This suggests that the rate of $CO_2$ storage in our experiments could have been enhanced if such high concentrations had been used. However, even though the rate was slower, MT2 experiment stored more $CO_2$ compared to Bobicki et al. (2015) and Garcia et al. (2010).

It is highly probable that the higher temperature range presumably limits carbonation, while the lower range limits $H_2$ production. The higher temperatures increase dissolution kinetics, leading to a larger amount of silica in solution. As that silica precipitates, they form secondary phyllosilicates that scavenge the divalent cations (equation 3). In contrast, the lower temperatures create lower silica supersaturation, and the cations enter carbonate phases leaving less iron available for oxidation and hydrogen production (equation

533 2). Nevertheless, this study proves that intermediate conditions can be set to make both

534 processes work simultaneously.

535     The amounts of hydrogen produced in our experiments were compared with two

536 similar studies (Crouzet et al., 2017; Malvoisin et al., 2013), who attempted to produce

537 hydrogen by using pure wüstite (FeO) and Fe-rich steel slag (Table 5). For the sake of

538 comparison, hydrogen produced at 473 K or 573 K, and 30 MPa after ca. 69 or 160 hours of

539 each study were used. The study by Malvoisin et al. (2013) used a carbonated basic oxygen

540 furnace (CARBOF) containing 2.7 wt.% Fe(0), 20.58 wt.% FeO and 3.16 wt.% $Fe_2O_3$. The

541 grain size of original steel slag used for carbonation was 1 -50 μm. The second study (Crouzet

542 et al., 2017) is a follow-up study of Malvoisin et al. (2013) that investigates the hydrogen

543 production under acidic pH conditions using 50-100 μm size pure wüstite (FeO). Because the

544 chemical composition of steel slag, wüstite and New Caledonian mine tailings largely differ

545 from each other, we calculated the hydrogen production per mass unit of FeO of each

546 material. In our study, the hydrogen measured by gas chromatography, and average FeO in

547 mine tailings (12.95 wt.%) were used for this calculation.

548     As shown in Table 5, $H_2$ production seems to be correlated with pH: the lower it is, the

549 higher the amount of $H_2$ generated. This can be explained by the fact that low pH promotes

550 mineral dissolution and thus $Fe^{2+}$ release. Thus, at a similar temperature (573K), this study

551 (pH 3.9) generates more $H_2$ than Crouzet (pH 6.0), which generates more than Malvoisin (pH

552 6.9). However, the pH effect is not the only way to increase $H_2$ production. As shown by

553 Crouzet et al. (2017), the addition of organic ligands (such as acetic acid) can increase $H_2$

554 generation even further by promoting mineral dissolution.

555

**4.5 Implications for $CO_2$ sequestration and hydrogen production in New Caledonian mining sites and other Ni mining sites**

New Caledonia is the 11th largest Ni producer in the world, preceded by the United states, Australia, Brazil, Canada, China, Columbia, Cuba, Guatemala, Indonesia and Madagascar (U.S. Geological Survey, 2017). When scaled to land area, however, its production of Nickel is in the top 3, implying a high environmental fingerprint. In 2013, New Caledonia produced 127,027 metric tons (t) of nickel from 7.8 million metric tons (Mt) of saprolite ore and 36,839 t of nickel from 4.2 Mt of laterite ore, resulting approximately in 12 million metric tons (Mt) of mine tailings per year (Wacaster 2013). The management of mine tailings such as collection, storage and re-usage are costly to process. Currently these mine tailings are used for geo-technical aspects such as building roads, dams, and land filling. Compared to the traditional valorization methods, those proposed by this study are novel and might be used to contribute to today's always-increasing energy demands, by producing an energy source through waste recycling. In addition, implementing a simultaneous ex-situ $CO_2$ storage and hydrogen production plant in the vicinity of mining sites provides a safe and permanent disposal of $CO_2$ emitted by the nickel industry. Although the chemical looping processes have been documented for carbon capture and storage (Bui et al., 2018; Cormos, 2017), the idea of energy looping does not appear prominently in literature. It is nevertheless our belief that inspiration could be drawn from chemical looping: the energy needed for heating the material could be obtained passively by locating this plant near high temperature furnaces used for ore-processing.

The annual $CO_2$ emission of New Caledonia is about 4.3 Mt/y (Boden et al., 2017). Our experiments having shown that at 523 K and 30 MPa, mine tailings can trap at least 320 g of $CO_2$ per kg of mine tailings (supporting information S6), it follows that the

580    annual mine tailings production could potentially trap 3.8 Mt/y of $CO_2$, which represents

581    about 90% of New Caledonia's annual emissions.

582         The annual electrical consumption of New Caledonia is approximately 2400 GWh;

583    (New Caledonia Department of Energy, 2013). The maximum hydrogen production in our

584    experiments was 0.57 g hydrogen per kg of mine tailings at 573 K and 30 MPa. According to

585    this value, the annual mine tailings produced in New Caledonia is able to produce 6840 tons

586    of hydrogen per year, which is equivalent of generating 229 GWh/y (with $H_2$ combustion

587    generating around 120.5 MJ/kg or 33.5 kWh/kg). It represents around 10 % of New

588    Caledonia's annual electrical consumption. Furthermore, assuming an average family

589    consumes 3400 kWh/y (New Caledonia Department of Energy, 2013), the energy produced

590    would be sufficient to sustain around 67350 families.

591         One limiting factor regarding this method is the separation of small quantities of

592    hydrogen from $CO_2$ in the reactor. Separating $CO_2$ and $H_2$ from industrially important gas

593    mixtures (synthesis gas or natural gas) are widely performed using membrane methods

594    (Korelskiy et al., 2015). These membranes could be either made from polymers (Ghadimi et

595    al., 2014; Rabiee et al., 2014), or ceramic (Korelskiy et al., 2015), and they provide cost

596    effective means of separating gases in large scale.  In our opinion, a membrane method would

597    be suitable to separate hydrogen from $CO_2$ in this process.

598         We believe that the simultaneous application of ex-situ $CO_2$ sequestration and

599    hydrogen production using New Caledonian mine tailings could be easily applied to various

600    mining industries of mafic rocks, which presumably produce mine wastes of similar

601    compositional and mineralogical characteristics. By using the residual heat provided by a

602    third process such as the high temperature smelting of ore, those two processes could be

603    translated into a high-value, cost-effective industrial way of storing wastes and generating

604    clean energy.

## 5. Conclusions

Batch experiments conducted between 473 K - 573 K under high $pCO_2$ of 15-30 MPa have demonstrated the viability of using New Caledonian mine tailings in ex-situ carbonation process, while producing $H_2$ as a byproduct. The results suggest that mine tailings were altered into Fe-rich magnesite and phyllosilicates when reacted with $CO_2$-saturated water at the above mentioned conditions. We have outlined that the competition between Mg and Fe incorporation among the secondary phases seems to control the quantities of magnesite precipitation and hydrogen production. Taken together, these results suggest that the temperatures between 523 K and 540 K at $pCO_2$=30 MPa would be the most favorable conditions for reacting mine tailings in order to maintain both carbonation and hydrogen production in significant quantities.

This work suggest a method to treat New Caledonia's annual $CO_2$ emissions and energy demands cost-efficiently by recycling the heat used in metal extraction (>1273 K), providing a novel valorization method for New Caledonian mine tailings. This approach can be globally applied to nickel (Ni) mine tailings as well as other industrial waste materials containing Ca, Mg, and Fe; however we believe that the optimum P/T conditions might vary depending on the mineral composition and textural features of individual material.

43

628     review and constructive comments of the executive editor Prof. Michael Kersten and the

629     two anonymous reviewers are greatly appreciated.

## References

631     Abu-Jaber, N.S., Kimberley, M.M., 1992. Origin of ultramafic-hosted vein magnesite
632     deposits. Ore Geol. Rev. 7, 155–191. doi:10.1016/0169-1368(92)90004-5

633     Allen, D.E., Seyfried, W.E., 2003. Compositional controls on vent fluids from ultramafic-
634     hosted hydrothermal systems at mid-ocean ridges: An experimental study at 400° C, 500
635     bars. Geochim. Cosmochim. Acta. 67, 1531–1542. doi:10.1016/s0016-7037(02)01173-0

636     Andreani, M., Daniel, I., Pollet-Villard, M., 2012. Aluminum speeds up the hydrothermal
637     alteration of olivine. Am. Mineral. 98, 1738–1744. doi:10.2138/am.2013.4469

638     Barnes, C.S and Koretsky, M.., 2004. In engineering and chemical thermodynamics. John
639     Willey and Sons.

640     Béarat, H., McKelvy, M. J., Chizmeshya, A. V., Gormley, D., Nunez, R., Carpenter, R. W.,
641     ... & Wolf, G. H. (2006). Carbon sequestration via aqueous olivine mineral carbonation:
642     role of passivating layer formation. Environmental science & technology, 40(15), 4802-
643     4808.

644     Behar, F., Beaumont, V., De B. Penteado, H.L., 2001. Rock-Eval 6 technology:
645     Performances and developments. Oil Gas Sci. Technol. 56, 111–134.
646     doi:10.2516/ogst:2001013

647     Berndt, M.E., Allen, D.E., Seyfried, W.E., 1996. Reduction of $CO_2$ during serpentinization
648     of olivine at 300°C and 500 bar. Geology. 24, 351–354. doi:10.1130/0091
649     7613(1996)024<0351:ROCDSO>2.3.CO

650     Bish, D.L., Howard, S.A., 1988. Quantitative phase analysis using the Rietveld method. J.
651     Appl. Crystallogr. 21, 86–91. doi:10.1107/S0021889887009415

652     Bish, D.L., Post, J.E., 1993. Quantitative mineralogical analysis using the Rietveld full-
653     pattern fitting method. Am. Mineral. 78(9-10), 932-940.

654     Bobicki, E.R., Liu, Q., Xu, Z., Zeng, H., 2012. Carbon capture and storage using alkaline
655     industrial wastes. Prog. Energy Combust. Sci. doi:10.1016/j.pecs.2011.11.002

656     Bobicki, E. R., Liu, Q., & Xu, Z. (2015). Mineral carbon storage in pre-treated ultramafic
657     ores. Minerals Engineering, 70, 43-54.

658     Boden, T, Marland, G, and Andres, R., 2017. Global, Regional, and National Fossil-Fuel
659     $CO_2$ Emissions. Oak Ridge 3 National Laboratory, U.S. Department of Energy, Oak
660     Ridge, Tenn., U.S.A.

661     Bodénan, F., Bourgeois, F., Petiot, C., Augé, T., Bonfils, B., Julcour-lebigue, C., Guyot, F.,
662     2014. Ex situ mineral carbonation for $CO_2$ mitigation : Evaluation of mining waste
663     resources, aqueous carbonation processability and life cycle assessment ( Carmex project )
664     59, 52–63. doi:10.1016/j.mineng.2014.01.011

665     Brantley, S. L. (2003). Reaction kinetics of primary rock-forming minerals under ambient
666     conditions. Treatise on geochemistry, 5, 605.

667     Brunauer, S., Emmett, P.H., Teller, E., 1938. Adsorption of Gases in Multimolecular
668     Layer. J. Am. Chem. Soc. 60, 309–319. doi:citeulike-article-id:4074706

669     Bui, M., Adjiman, C. S., Bardow, A., Anthony, E. J., Boston, A., Brown, S., ... & Hallett,
670     J. P. (2018). Carbon capture and storage (CCS): the way forward. Energy &
671     Environmental Science.

672     Caesar, L., Rahmstorf, S., Robinson, A., Feulner, G., & Saba, V. (2018). Observed
673     fingerprint of a weakening Atlantic Ocean overturning circulation. Nature, 556(7700),
674     191.

675     Cormos, C. C. (2011). Hydrogen production from fossil fuels with carbon capture and
676     storage based on chemical looping systems. International journal of hydrogen energy,
677     36(10), 5960-5971.

678     Crouzet, C., Brunet, F., Recham, N., Findling, N., Lanson, M., Guyot, F., Ferrasse, J.H.,
679     Goffé, B., 2017. Hydrogen production by hydrothermal oxidation of FeO under acidic
680     conditions. Int. J. Hydrogen Energy 42, 795–806. doi:10.1016/j.ijhydene.2016.10.019

681     Daval, D., Martinez, I., Corvisier, J., Findling, N., Goffé, B., Guyot, F., 2009a.
682     Carbonation of Ca-bearing silicates, the case of wollastonite: Experimental investigations
683     and kinetic modeling. Chem. Geol. 262, 262–277. doi:10.1016/j.chemgeo.2009.01.022

684     Daval, D., Martinez, I., Guigner, J. M., Hellmann, R., Corvisier, J., Findling, N., ... &
685     Guyot, F. 2009b. Mechanism of wollastonite carbonation deduced from micro-to
686     nanometer length scale observations. American Mineralogist, 94(11-12), 1707-1726.

687     Ece, Ö.I., Matsubaya, O., Çoban, F., 2005. Genesis of hydrothermal stockwork-type
688     magnesite deposits associated with ophiolite complexes in the Kütahya-Eskişehir region,
689     Turkey. Neues Jahrb. für Mineral. - Abhandlungen 181, 191–205. doi:10.1127/0077-
690     7757/2005/0014

691     Edenhofer, O., Pichs-Madruga, R. Sokona, Y., Farahani, E., Kadner, S., Seyboth, K.,
692     Adler, A., Baum, I., Brunner, S., Eickemeier, P., Kriemann, B., Savolainen, J., Schlömer,
693     S., von Stechow, C., Zwickel, T., Minx, J.C., 2014. IPCC, 2014. Summary for
694     policymakers, climate change 2014: mitigation of climate change. Contribution of
695     working group iii to the fifth assessment report of the intergovernmental panel on climate
696     change. doi:10.1007/s13398-014-0173-7.2

697    Garcia, B., Beaumont, V., Perfetti, E., Rouchon, V., Blanchet, D., Oger, P., Dromart, G.,
698    Huc, A.Y., Haeseler, F., 2010. Experiments and geochemical modelling of $CO_2$
699    sequestration by olivine: Potential, quantification. Appl. Geochemistry 25, 1383–1396.
700    doi:10.1016/j.apgeochem.2010.06.009

701    Gerdemann, S.J., O'Connor, W.K., Dahlin, D.C., Penner, L.R., Rush, H., 2007. Ex situ
702    aqueous mineral carbonation. Environ. Sci. Technol. 41, 2587–2593.
703    doi:10.1021/es0619253

704    Ghadimi, A., Amirilargani, M., Mohammadi, T., Kasiri, N., Sadatnia, B., 2014.
705    Preparation of alloyed poly(ether block amide)/poly(ethylene glycol diacrylate)
706    membranes for separation of $CO_2/H_2$(syngas application). J. Memb. Sci. 458, 14–26.
707    doi:10.1016/j.memsci.2014.01.048

708    Golubev, S. V., Pokrovsky, O. S., & Schott, J. (2005). Experimental determination of the
709    effect of dissolved CO2 on the dissolution kinetics of Mg and Ca silicates at 25 C.
710    Chemical Geology, 217(3-4), 227-238.

711    Gudbrandsson, S., Wolff-Boenisch, D., Gislason, S.R., Oelkers, E.H., 2011. An
712    experimental study of crystalline basalt dissolution from 2pH11 and temperatures from 5
713    to 75°C. Geochim. Cosmochim. Acta. 75, 5496–5509. doi:10.1016/j.gca.2011.06.035

714    Guthrie, G. (2001). Geochemical aspects of the carbonation of magnesium silicates in an
715    aqueous medium (No. LA-UR-01-1429). Los Alamos National Lab., NM (US).

716    Guyot, F., Daval, D., Dupraz, S., Martinez, I., Ménez, B., Sissmann, O., 2011. $CO_2$
717    geological storage: The environmental mineralogy perspective. Comptes Rendus Geosci.
718    343, 246–259. doi:10.1016/j.crte.2010.12.007

719    Harrison, A.L., Dipple, G.M., Power, I.M., Mayer, K.U., 2016. The impact of evolving
720    mineral-water-gas interfacial areas on mineral-fluid reaction rates in unsaturated porous
721    media. Chem. Geol. 421, 65–80. doi:10.1016/j.chemgeo.2015.12.005

722    Harrison, A.L., Power, I.M., Dipple, G.M., 2013. Accelerated carbonation of brucite in
723    mine tailings for carbon sequestration. Environ. Sci. Technol. 47, 126–134.
724    doi:10.1021/es3012854

725    Janecky, D.R., Seyfried, W.E., 1986. Hydrothermal serpentinization of peridotite within
726    the oceanic crust: Experimental investigations of mineralogy and major element
727    chemistry. Geochim. Cosmochim. Acta. 50, 1357–1378. doi:10.1016/0016-
728    7037(86)90311-X

729    Ji, S., Zhu, J., He, H., Tao, Q., Zhu, R., Ma, L., ... & Zhou, J. (2018). Conversion of
730    serpentine to smectite under hydrothermal condition: Implication for solid-state
731    transformation. American Mineralogist, 103(2), 241-251.

Johnson, N. C., Thomas, B., Maher, K., Rosenbauer, R. J., Bird, D., & Brown Jr, G. E. (2014). Olivine dissolution and carbonation under conditions relevant for in situ carbon storage. Chemical Geology, 373, 93-105.

King, H. E., Plümper, O., & Putnis, A. (2010). Effect of secondary phase formation on the carbonation of olivine. Environmental science & technology, 44(16), 6503-6509.

Klein, F., Bach, W., Jöns, N., McCollom, T., Moskowitz, B., Berquó, T., 2009. Iron partitioning and hydrogen generation during serpentinization of abyssal peridotites from 15°N on the Mid-Atlantic Ridge. Geochim. Cosmochim. Acta. 73, 6868–6893. doi:10.1016/j.gca.2009.08.021

Klein, F., Bach, W., McCollom, T.M., 2013. Compositional controls on hydrogen generation during serpentinization of ultramafic rocks. Lithos. 178, 55–69. doi:10.1016/j.lithos.2013.03.008

Klein, F., Garrido, C.J., 2010. On Serpentinization and Mineral Carbonation of Serpentinite. In AGU Fall Meeting Abstracts. Am. Geophys. Union.

Kondo, M., Ichii, K., Patra, P. K., Canadell, J. G., Poulter, B., Sitch, S., ... & Saigusa, N. (2018). Land use change and El Niño-Southern Oscillation drive decadal carbon balance shifts in Southeast Asia. Nature communications, 9.

Lackner, K.S., Wendt, C.H., Butt, D.P., Joyce, E.L., Sharp, D.H., 1995. Carbon-dioxide disposal in carbonate minerals. Energy. 20, 1153–1170. doi:10.1016/0360-5442(95)00071-n

Lafargue, E., Marquis, F., Pillot, D., 1998. Rock-Eval 6 applications in hydrocarbon exploration, production, and soil contamination studies. Oil Gas Sci. Technol. 53, 421–437. doi:10.2516/ogst:1998036

Lugli, S., Torres-Rutz, J., Garuti, G., Olmedo, F., 2000. Petrography and geochemistry of the Eugui magnesite deposit (Western Pyrenees, Spain): evidence for the development of a peculiar zebra banding by dolomite replacement. Econ. Geol. 95(8), 1775-1791. doi:10.2113/gsecongeo.95.8.1775

Malvoisin, B., Brunet, F., Carlut, J., Montes-Hernandez, G., Findling, N., Lanson, M., Vidal, O., Bottero, J.Y., Goff, B., 2013. High-purity hydrogen gas from the reaction between BOF steel slag and water in the 473-673 K range. Int. J. Hydrogen Energy. 38, 7382–7393. doi:10.1016/j.ijhydene.2013.03.163

Malvoisin, B., Brunet, F., Carlut, J., Rouméjon, S., Cannat, M., 2012a. Serpentinization of oceanic peridotites: 2. Kinetics and processes of San Carlos olivine hydrothermal alteration. J. Geophys. Res. Solid Earth. 117, 1–13. doi:10.1029/2011JB008842

Malvoisin, B., Carlut, J., Brunet, F., 2012b. Serpentinization of oceanic peridotites: 1. A high-sensitivity method to monitor magnetite production in hydrothermal experiments. J. Geophys. Res. Solid Earth 117. doi:10.1029/2011JB008612

769  Manabe, S., Stouffer, R.J., 1993. Century-scale effects of increased atmospheric $CO_2$ on
770  the ocean-atmosphere system. Nature 364, 215–218. doi:10.1038/364215a0

771  Marcaillou, C., Muñoz, M., Vidal, O., Parra, T., Harfouche, M., 2011a. Mineralogical
772  evidence for $H_2$ degassing during serpentinization at 300°C/300bar. Earth Planet. Sci.
773  Lett. 303, 281–290. doi:10.1016/j.epsl.2011.01.006

774  Marzeion, B., Kaser, G., Maussion, F., & Champollion, N. (2018). Limited influence of
775  climate change mitigation on short-term glacier mass loss. Nature Climate Change, 8(4),
776  305.

777  Matter, J.M., Kelemen, P.B., 2009. Permanent storage of carbon dioxide in geological
778  reservoirs by mineral carbonation. Nat. Geosci. 2, 837–841. doi:10.1038/ngeo683

779  Matter, J.M., Stute, M., Hall, J., Mesfin, K., Snæbjörnsdóttir, S., Gislason, S.R., Oelkers,
780  E.H., Sigfusson, B., Gunnarsson, I., Aradottir, E.S., Alfredsson, H.A., Gunnlaugsson, E.,
781  Broecker, W.S., 2014. Monitoring permanent $CO_2$ storage by in situ mineral carbonation
782  using a reactive tracer technique, in: Energy Procedia. pp. 4180–4185.
783  doi:10.1016/j.egypro.2014.11.450

784  McCollom, T.M., Bach, W., 2009a. Thermodynamic constraints on hydrogen generation
785  during serpentinization of ultramafic rocks. Geochim. Cosmochim. Acta. 73, 856–875.
786  doi:10.1016/j.gca.2008.10.032

787  McCollom, T.M., Bach, W., 2009b. Thermodynamic constraints on hydrogen generation
788  during serpentinization of ultramafic rocks. Geochim. Cosmochim. Acta. 73, 856–875.
789  doi:10.1016/j.gca.2008.10.032

790  McCollom, T.M., Klein, F., Robbins, M., Moskowitz, B., Berquó, T.S., Jöns, N., Bach, W.,
791  Templeton, A., 2016. Temperature trends for reaction rates, hydrogen generation, and
792  partitioning of iron during experimental serpentinization of olivine. Geochim.
793  Cosmochim. Acta. 181, 175–200. doi:10.1016/j.gca.2016.03.002

794  McCollom, T.M., Seewald, J.S., 2001. A reassessment of the potential for reduction of
795  dissolved $CO_2$ to hydrocarbons during serpentinization of olivine. Geochim. Cosmochim.
796  Acta. 65, 3769–3778. doi:10.1016/S0016-7037(01)00655-X

797  McCusker, L.B., Von Dreele, R.B., Cox, D.E., Louër, D., Scardi, P., 1999. Rietveld
798  refinement guidelines. J. Appl. Crystallogr. 32, 36–50. doi:10.1107/S0021889898009856

799  McMollom, T.M., Bach, W., 2008. Constraints on hydrogen generationduring
800  serpentinization of ultramaficrocks. Geochim. Cosmochim. Acta 72, A611.

801  New Caledonia Department of Energy, 2013. Bilan energetique de la nouvelle-caledonie-
802  2013. Retrieved from https://maitrise-
803  energie.nc/sites/default/files/documents/bilan_energetique_2013.pdf

804      NOAA, 2016. Trends in Atmospheric Carbon Dioxide. Retrieved from
805      http://www.esrl.noaa.gov/gmd/ccgg/trends/.

806      O'Connor, W. K., Dahlin, D. C., Turner, P. C., & Walters, R. P. 2000. Carbon dioxide
807      sequestration by ex-situ mineral carbonation (No. DOE/ARC-1999-009). Albany Research
808      Center (ARC), Albany, OR.

809      Oelkers, E.H., 2005. Geochemical aspects of $CO_2$ sequestration. Chem. Geol. 217, 183–
810      186. doi:10.1016/j.chemgeo.2004.12.006

811      Oskierski, H.C., Dlugogorski, B.Z., Jacobsen, G., 2013. Sequestration of atmospheric $CO_2$
812      in a weathering-derived, serpentinite-hosted magnesite deposit: $^{14}C$ tracing of carbon
813      sources and age constraints for a refined genetic model. Geochim. Cosmochim. Acta. 122,
814      226–246. doi:10.1016/j.gca.2013.08.029

815      Palinkaš, L.A., Jurković, I., Garašić, V., Palinkaš, S.S., 2012. Genesis of vein-stockwork
816      cryptocrystalline magnesite from the dinaride ophiolites. Ofioliti. 37, 13–26.

817      Park, A. H. A., Jadhav, R., & Fan, L. S. (2003). CO2 mineral sequestration: chemically
818      enhanced aqueous carbonation of serpentine. The Canadian Journal of Chemical
819      Engineering, 81(3‐4), 885-890.

820      Power, I.M., Harrison, A.L., Dipple, G.M., Wilson, S.A., Kelemen, P.B., Hitch, M.,
821      Southam, G., 2013. Carbon Mineralization: From Natural Analogues to Engineered
822      Systems. Rev. Mineral. Geochemistry 77, 305–360. doi:10.2138/rmg.2013.77.9

823      Rabiee, H., Soltanieh, M., Mousavi, S.A., Ghadimi, A., 2014. Improvement in $CO_2/H_2$
824      separation by fabrication of poly(ether-b-amide6)/glycerol triacetate gel membranes. J.
825      Memb. Sci. 469, 43–58. doi:10.1016/j.memsci.2014.06.026

826      Seifritz, W., 1990. $CO_2$ disposal by means of silicates. Nature. 345(6275), 486.
827      doi:10.1038/345486b0

828      Seyfried, W.E., Foustoukos, D.I., Fu, Q., 2007. Redox evolution and mass transfer during
829      serpentinization: An experimental and theoretical study at 200°C, 500bar with
830      implications for ultramafic-hosted hydrothermal systems at Mid-Ocean Ridges. Geochim.
831      Cosmochim. Acta. 71, 3872–3886. doi:10.1016/j.gca.2007.05.015

832      Sissmann, O., Brunet, F., Martinez, I., Guyot, F., Verlaguet, A., Pinquier, Y., Daval, D.,
833      2014. Enhanced olivine carbonation within a basalt as compared to single-phase
834      experiments: Reevaluating the potential of $CO_2$ mineral sequestration. Environ. Sci.
835      Technol. 48, 5512–5519. doi:10.1021/es405508a

836      Sissmann, O., Daval, D., Brunet, F., Guyot, F., Verlaguet, A., Pinquier, Y., Findling, N.,
837      Martinez, I., 2013. The deleterious effect of secondary phases on olivine carbonation
838      yield: Insight from time-resolved aqueous-fluid sampling and FIB-TEM characterization.
839      Chem. Geol. 357, 186–202. doi:10.1016/j.chemgeo.2013.08.031

840     Snæbjörnsdóttir, S., Oelkers, E.H., Mesfin, K., Aradóttir, E.S., Dideriksen, K.,
841     Gunnarsson, I., Gunnlaugsson, E., Matter, J.M., Stute, M., Gislason, S.R., 2017. The
842     chemistry and saturation states of subsurface fluids during the in situ mineralisation of
843     $CO_2$ and $H_2S$ at the CarbFix site in SW-Iceland. Int. J. Greenh. Gas Control 58, 87–102.
844     doi:10.1016/j.ijggc.2017.01.007

845     Takahashi, E., 1986. Melting of a dry peridotite KLB-1 up to 14 GPa: Implications on the
846     Origin of peridotitic upper mantle. J. Geophys. Res. 91, 9367–9382.
847     doi:10.1029/JB091iB09p09367

848     U.S. Geological Survey, 2017. Mineral Commodity Summaries 2017.

849     van der Lee, J and De Windt, L., 2002. CHESS tutorial and cookbook updated for version
850     3.0. Ecole des Mines de Paris, Fontainebleau, France.

851     Wacaster, S., 2013. Minerals Yearbook New Caledonia (advance release). U.S. Geological
852     survey.

853     Wilson, S.A., Harrison, A.L., Dipple, G.M., Power, I.M., Barker, S.L.L., Ulrich Mayer, K.,
854     Fallon, S.J., Raudsepp, M., Southam, G., 2014. Offsetting of $CO_2$ emissions by air capture
855     in mine tailings at the Mount Keith Nickel Mine, Western Australia: Rates, controls and
856     prospects for carbon neutral mining. Int. J. Greenh. Gas Control. 25, 121–140.
857     doi:10.1016/j.ijggc.2014.04.002

858     Wolff-Boenisch, D., Gislason, S. R., & Oelkers, E. H. (2006). The effect of crystallinity
859     on dissolution rates and CO2 consumption capacity of silicates. Geochimica et
860     Cosmochimica Acta, 70(4), 858-870.

861     Wolff-Boenisch, D., Wenau, S., Gislason, S. R., & Oelkers, E. H. (2011). Dissolution of
862     basalts and peridotite in seawater, in the presence of ligands, and $CO_2$: Implications for
863     mineral sequestration of carbon dioxide. Geochimica et Cosmochimica Acta, 75(19),
864     5510-5525.

865     Zhang, X., Knorr, G., Lohmann, G., & Barker, S. (2017). Abrupt North Atlantic
866     circulation changes in response to gradual CO 2 forcing in a glacial climate state. Nature
867     Geoscience, 10(7), 518.

868     Zedef, V., Russell, M.J., Fallick, A.E., Hall, A.J., 2000. Genesis of vein stockwork and
869     sedimentary magnesite and hydromagnesite deposits in the ultramafic terranes of
870     southwestern Turkey: A stable isotope study. Econ. Geol. 95, 429–445.
871     doi:10.2113/gsecongeo.95.2.429

872

874 **Simultaneous ex-situ CO$_2$ mineral sequestration and H$_2$ production from New**

875 **Caledonian mine tailings**

876 Kanchana Kularatne[a,b (*)], Olivier Sissmann[a], Eric Kohler[a], Michel Chardin[a], Sonia Noirez[a],

877 Isabelle Martinez[b]

878 [a]IFP Energies Nouvelles, 1- 4 Avenue du Bois Préau, 92852 Rueil-Malmaison, France

879 [b]Institut de Physique du Globe de Paris, Sorbonne Paris Cité, Université Paris Diderot, UMR

880 7154 CNRS, 1 rue Jussieu, F-75005 Paris, France

881 **Gas phase data**

882 S1.The composition of gas phase of MT1 experiment conducted at 473 K and 15 MPa.

| MT1 | | | | | |
|---|---|---|---|---|---|
| **Duration** | **H2** | **CH4** | **CO2** | **N2** | **O2** |
| **(days)** | **(µmols/g)** | **(µmols/g)** | **(mmols/g)** | **(mmols/g)** | **(mmols/g)** |
| 0.1 | 4.54 | - | 94.6 | 0.24 | 0.04 |
| 0.9 | 1.44 | - | 94.0 | 3.84 | 0.99 |
| 1.8 | 1.35 | - | 91.0 | 7.98 | 2.02 |
| 2.8 | 4.76 | - | 106.8 | - | - |
| 5.8 | 6.62 | - | 113.8 | 0.24 | 0.04 |
| 7.8 | 5.94 | - | 119.1 | - | - |
| 8.8 | 8.42 | - | 127.0 | - | - |
| 9.8 | 8.01 | 0.17 | 130.9 | - | - |
| 13.0 | 0.21 | - | 136.4 | - | - |
| 13.8 | 6.11 | 0.24 | 143.0 | - | - |
| 16.0 | 16.92 | 0.23 | 149.3 | - | - |
| 20.0 | 15.20 | 0.27 | 154.1 | - | - |
| 22.8 | 17.87 | - | 159.8 | - | - |
| 23.8 | 19.99 | - | 165.9 | 0.05 | - |

883

884    S2. The composition of gas phase of MT2 experiment conducted at 523 K and 30 MPa.

| MT2 | | | | | | | | | |
|------|------|------|------|------|------|------|------|------|------|
| Duration | H2 | CH4 | CO2 | N2 | O2 | C2H6 | C3H8 | iC4H10 | nC4H11 |
| (days) | (μmols/g) | (μmols/g) | (mmols/g) | (mmols/g) | (mmols/g) | (μmols/g) | (μmols/g) | (μmols/g) | (μmols/g) |
| 0.00 | 0.00 | 0.00 | 179.13 | 0.13 | 0.02 | - | - | - | - |
| 0.69 | 0.00 | 0.43 | 184.38 | 0.18 | - | - | - | - | - |
| 0.96 | 0.00 | 5.71 | 189.23 | 0.18 | - | - | - | - | - |
| 1.71 | 0.00 | 0.44 | 195.42 | 0.18 | - | - | - | - | - |
| 1.96 | 3.48 | 0.21 | 200.97 | - | - | - | - | - | - |
| 4.68 | 2.79 | 0.22 | 206.68 | 0.17 | 0.19 | - | - | - | - |
| 5.88 | 5.64 | 0.65 | 211.31 | 0.29 | 0.03 | - | - | - | - |
| 6.68 | 7.67 | 1.44 | 215.93 | 0.61 | 0.11 | - | - | - | - |
| 7.72 | 6.52 | 0.76 | 228.60 | 0.46 | 0.04 | - | - | - | - |
| 8.92 | 8.37 | 0.75 | 228.11 | 0.23 | - | - | - | - | - |
| 11.71 | 43.67 | 4.82 | 231.46 | 0.24 | - | 0.41 | 0.59 | 0.04 | 1.27 |
| 13.71 | 47.75 | 12.33 | 228.82 | 6.52 | 1.46 | 4.01 | 1.93 | 0.36 | 2.23 |
| 14.71 | 37.48 | 3.59 | 242.22 | 0.25 | - | - | 0.38 | 0.03 | 0.72 |
| 18.71 | 53.80 | 2.56 | 247.42 | 0.40 | 0.04 | - | 0.42 | - | 0.67 |
| 20.75 | 117.57 | 5.94 | 253.49 | 0.64 | 0.09 | - | 0.58 | 0.03 | 0.99 |
| 22.75 | 58.49 | 1.41 | 258.83 | - | - | - | - | - | - |
| 25.76 | 76.69 | 2.00 | 263.83 | - | - | - | - | - | - |

885

886

887

35

888    S3.The composition of gas phase of MT4 experiment conducted at 573 K and 30 MPa.

| MT4 | | | | | | | | | |
|---|---|---|---|---|---|---|---|---|---|
| Duration | H2 | CH4 | CO2 | N2 | O2 | C2H6 | C3H8 | iC4H10 | nC4H11 |
| (days) | (μmols/g) | (μmols/g) | (mmols/g) | (mmols/g) | (mmols/g) | (μmols/g) | (μmols/g) | (μmols/g) | (μmols/g) |
| 0 | 0.00 | 0.10 | 183.56 | 0.38 | 0.10 | - | - | - | - |
| 0.76 | 116.17 | 9.93 | 146.34 | 0.78 | 0.15 | - | 0.82 | - | 1.89 |
| 1.13 | 106.77 | 11.32 | 147.27 | 4.92 | 1.14 | - | 1.95 | 0.09 | 2.89 |
| 1.80 | 0.00 | 0.47 | 200.07 | 2.47 | 0.47 | - | - | - | - |
| 2.85 | 186.29 | 26.19 | 138.04 | 22.60 | - | 3.70 | 10.72 | 0.60 | 11.08 |
| 4.04 | 0.00 | 1.76 | 208.04 | 3.71 | 0.93 | - | - | - | - |
| 6.83 | 145.06 | 1.73 | 219.28 | - | - | - | - | - | - |
| 8.83 | 283.50 | 1.22 | 226.74 | - | - | - | - | - | - |
| 9.88 | 35.97 | 8.47 | 230.83 | 1.40 | 0.17 | 0.79 | 2.12 | 0.10 | 2.87 |
| 13.83 | 73.78 | 5.85 | 238.71 | 0.20 | 0.02 | - | 0.45 | 0.04 | 1.40 |
| 15.88 | 41.76 | 4.72 | 245.09 | 0.15 | 0.01 | - | 0.37 | 0.30 | 0.73 |
| 17.88 | 48.17 | 5.49 | 249.76 | 0.16 | 0.01 | - | - | 0.19 | 0.71 |
| 20.88 | 21.94 | 1.88 | 245.44 | - | - | - | - | - | - |
| 24.01 | 41.18 | 24.14 | 247.30 | 0.50 | 0.12 | 8.16 | 16.95 | 0.74 | 14.76 |

889

890

891

892

893 S4. The composition of gas phase of MT2b experiment conducted at 523 K and 30 MPa. This is a blank experiment conducted at similar PT

894 conditions in comparison with MT2, without introducing mine tailings in the reactor (due to technical difficulties, CO2 was not readjusted after

895 the first sampling).

| MT2b | | | | | | | | | |
|---|---|---|---|---|---|---|---|---|---|
| Duration | H2 | CH4 | CO2 | N2 | O2 | C2H6 | C3H8 | iC4H10 | nC4H11 |
| (days) | (μmols/g) | (μmols/g) | (mmols/g) | (mmols/g) | (mmols/g) | (μmols/g) | (μmols/g) | (μmols/g) | (μmols/g) |
| 7.21 | - | 0.15 | 280.94 | 0.10 | - | - | - | - | - |
| 19.17 | - | 2.42 | 192.34 | 0.19 | 0.03 | 1.67 | 7.28 | 0.81 | 12.16 |
| 24.17 | - | 3.81 | 197.10 | 0.20 | 0.02 | 2.05 | 8.37 | 1.17 | 16.95 |

896

897

898

899

900

901

902 S5.The composition of gas phase of MT4b experiment conducted at 573 K and 30 MPa. This is a blank experiment without reactants in order to

903 monitor H2 and CH4 concentrations. It was conducted at similar PT conditions in comparison with MT4, without introducing mine tailings in the

904 reactor (due to technical difficulties, CO2 was not readjusted after the first sampling).

| MT4b Duration (days) | H2 (μmols/g) | CH4 (μmols/g) | CO2 (mmols/g) | N2 (mmols/g) | O2 (mmols/g) | C2H6 (μmols/g) | C3H8 (μmols/g) | iC4H10 (μmols/g) | nC4H11 (μmols/g) |
|---|---|---|---|---|---|---|---|---|---|
| 7.21 | - | 7.44 | 280.58 | - | - | 2.51 | 6.02 | 0.30 | 7.30 |
| 19.17 | - | 7.76 | 191.52 | 0.33 | 0.16 | 6.72 | 26.92 | 3.55 | 52.42 |
| 24.17 | - | 7.49 | 195.13 | 0.29 | 0.13 | 4.29 | 13.39 | 1.84 | 28.87 |

905

906 **Quantification of secondary phases**

907 **S6. Calculation of carbonate yield**

908 The quantification of carbonate phases using Rock-Eval 6 (Behar et al., 2001) involves

909 pyrolysis and oxidation of ~40 mg of sample in an inert gas flow above 400 °C and oxidation

910 at temperatures between 650°C–850°C. The gaseous $CO_2$ produced during the pyrolysis and

911 oxidation cycles is analyzed by an infra-red analyzer (eg; S3' peak and S5 peak respectively)

912 in online mode and the peak areas of S3' and S5 peaks are used to calculate the percent

913 weight of carbonate according to the equations,

914

915 PyroMinC (wt.%)= [[S3^'* 12/44]+[S3'CO/2]*12/28]/10

916 OxiMinC (wt.%)= [S5*12/44]/10

917 The amount of total mineral carbon (MinC) in the sample is obtained by the addition of

918 weight percent (wt.%) of mineral carbon produced from pyrolysis cycle (PyroMinC) and

919 oxidation cycle (OxyMinC) as below,

920 MinC (wt.%) = PyoMinC + OxyMinC

921 wt% $_{Carbonate}$ = MinC x($M_{carbonate}$ / $M_{carbon}$) , where the molar mass of carbon is 12 g/mol the

922 molar mass of carbonates is :

923    -   for MT1 M (($Mg_{0.92}Fe_{0.08}$)$CO_3$) = 86.8 g/mol

924    -   for MT2 M (($Mg_{0.58}Fe_{0.42}$)$CO_3$) = 97.53 g/mol

925    -   for MT4 M (($Mg_{0.83}Fe_{0.17}$)$CO_3$) = 89.7 g/mol

926

927    -

| | MinC | M carbonate g/mol | wt% Carbonate | m Carbonate g/kg | n Carbonate mol/kg | n CO₂ mol/kg | m CO2 g/kg |
|------|------|------|------|------|------|------|------|
| MT1 | 2.8 | 86.8 | 20.3% | 225.7 | 2.60 | 2.60 | 114.4 |
| MT2 | 6.62 | 97.5 | 53.8% | 710.5 | 7.28 | 7.28 | 320.5 |
| MT4 | 2.89 | 89.7 | 21.6% | 241.6 | 2.69 | 2.69 | 118.5 |

928    Calculations for the amount of $CO_2$ trapped can be performed as follows :

$$m_{CO2\ trapped} = \frac{M_{CO2}}{M_{carbonate}} \times m_{carbonate}$$

$$m_{CO2\ trapped} = \frac{M_{CO2}}{M_{carbonate}} \times (wt\%_{carbonate} \times m_{run\ products})$$

$$m_{CO2\ trapped} = \frac{M_{CO2}}{M_{carbonate}} \times wt\%_{carbonate} \times (m_{0\ mine\ tailings} + m_{CO2\ trapped})$$

929    e.g. for MT2 :    $m_{CO2\ trapped} = \frac{44}{97.53} \times 53.8\ \% \times (2\ g + m_{CO2\ trapped})$

$$m_{CO2\ trapped} = 0.485\ g + (0.243 \times m_{CO2\ trapped})$$

$$m_{CO2\ trapped} = 0.485\ g + (0.243 \times m_{CO2\ trapped})$$

$$m_{CO2\ trapped} = 0.641\ g\ for\ 2\ g\ of\ mine\ tailings)$$

$$m_{CO2\ trapped} = 320\ g\ for\ 1\ kg\ of\ mine\ tailings$$

930

931

932

933

934

935

**SEM analysis on reaction products**

937 **S7.** SEM images of the ionically polished sections of experimental product at T = 473 K and P

938 = 15 MPa showing large anhedral magnesite crystals grown around glass (gl) and olivine (ol).

939 Secondary phyllosilicates (phy) layers around glass. (b) magnified image of yellow square

940 marked on (a); (c) glass altered into magnesite; The chemical composition of phyllosilicate,

941 magnesite, olivine and glass analyzed by SEM-EDX are shown in the pie charts.



942
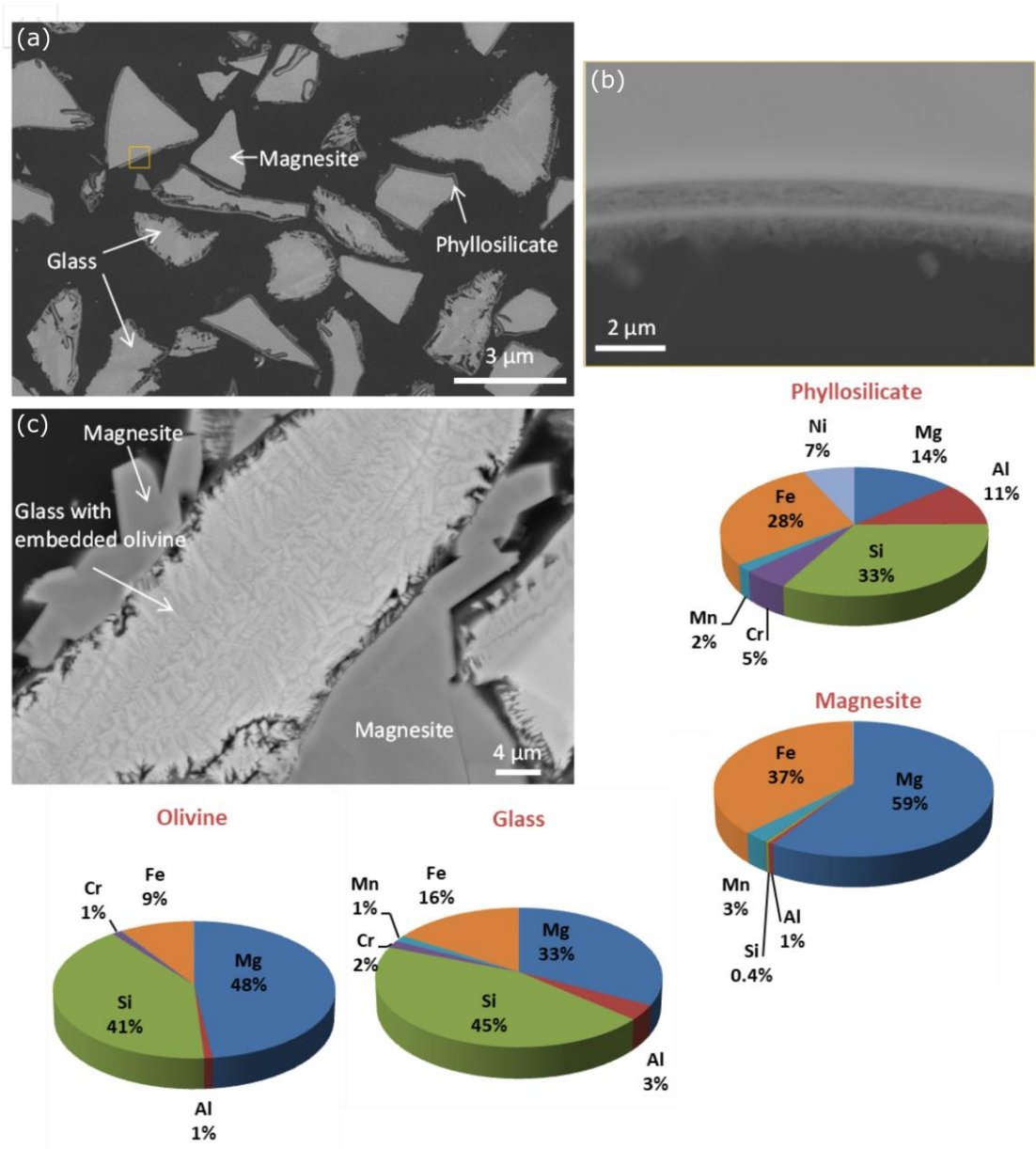
943 **S8.** SEM images of the ionically polished sections of experimental product at T = 523 K and P =

944 30 MPa showing euhedral magnesite crystals and secondary phyllosilicates. (b) a magnified view

945 of phyllosilicate (c) SEM image of a polished section of the products showing magnesite with

946 zoning. The chemical composition obtained by SEM EDX analysis is shown in pie charts.



947

948

949
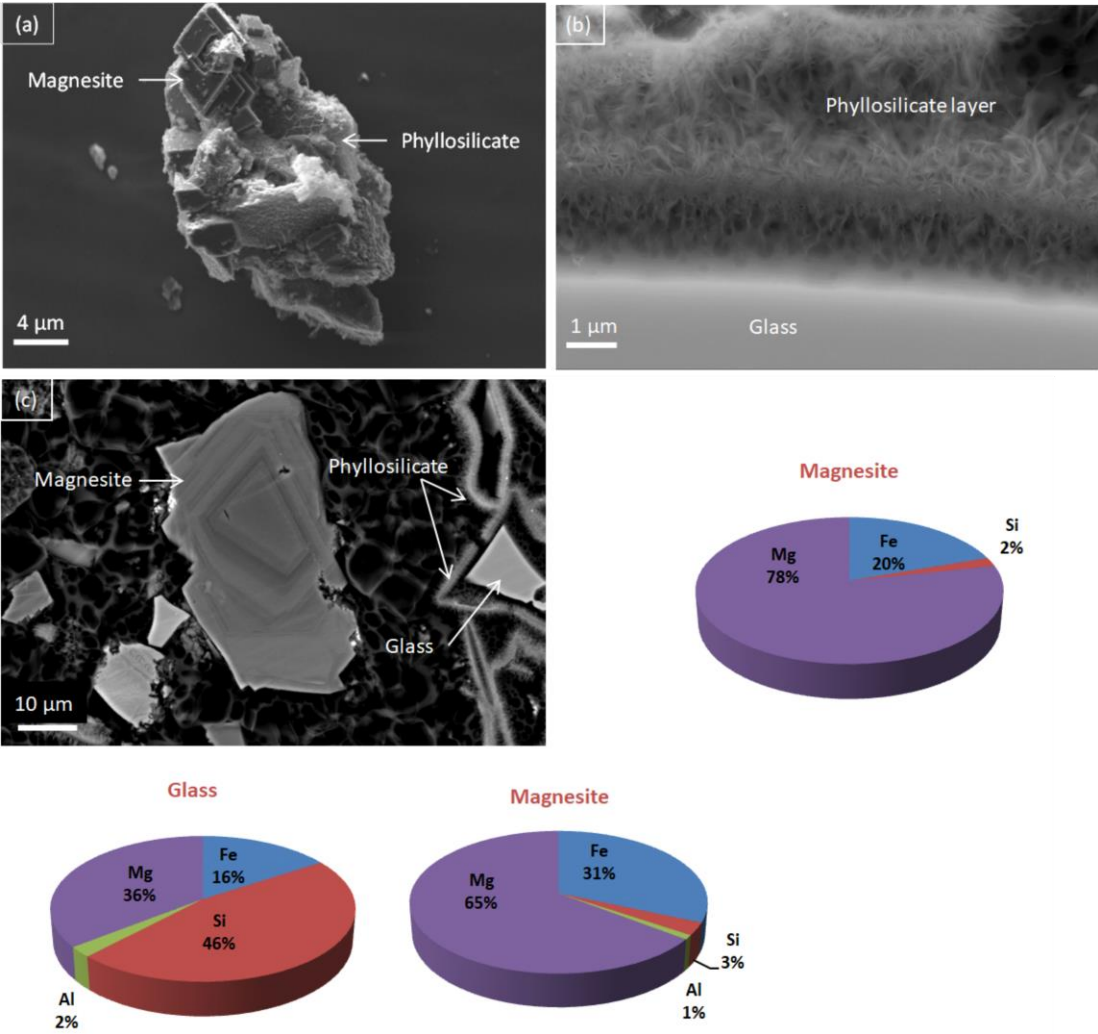
950 S9. SEM images of the ionically polished sections of experimental product at T = 573 K and P =

951 30 MPa, showing anhedral magnesite formed around glass, and heavily altered glass with thick

952 layers of phyllosilicate.
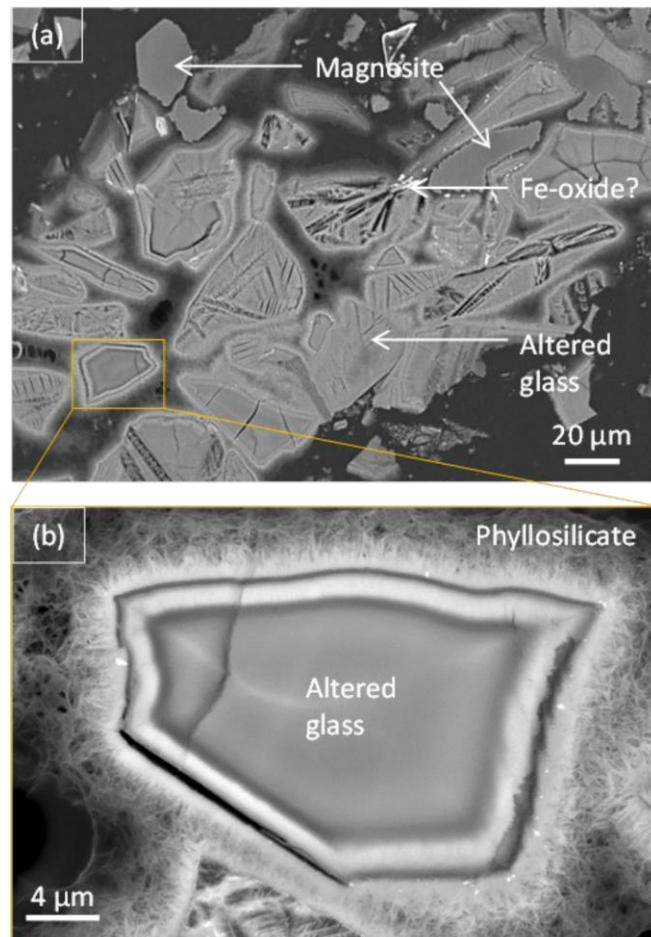


953

954

955

956

957

958 **S10.** FIB –TEM analysis

959 Ultra-thin, electron transparent (<200 nm) sections of each solid reaction product was prepared

960 by performing FIB milling at IPGP and also at Institute of Electronics, Microelectronics and

961 Nanotechnology (IEMN), Lille using a gallium (Ga) beam. These sections which are thinned

962 down to electron transparency (<200 nm) were then analyzed using transmission electron

963 microscopy (TEM). For this study, we only used the composition of magnesite obtained by the

964 TEM-EDX analysis, and the detailed mineralogical analysis of other phases, in order to

965 understand the mineral-water interactions, is still on going.

966

967 **S11.** Calculation of maximum carbonation of mine tailings

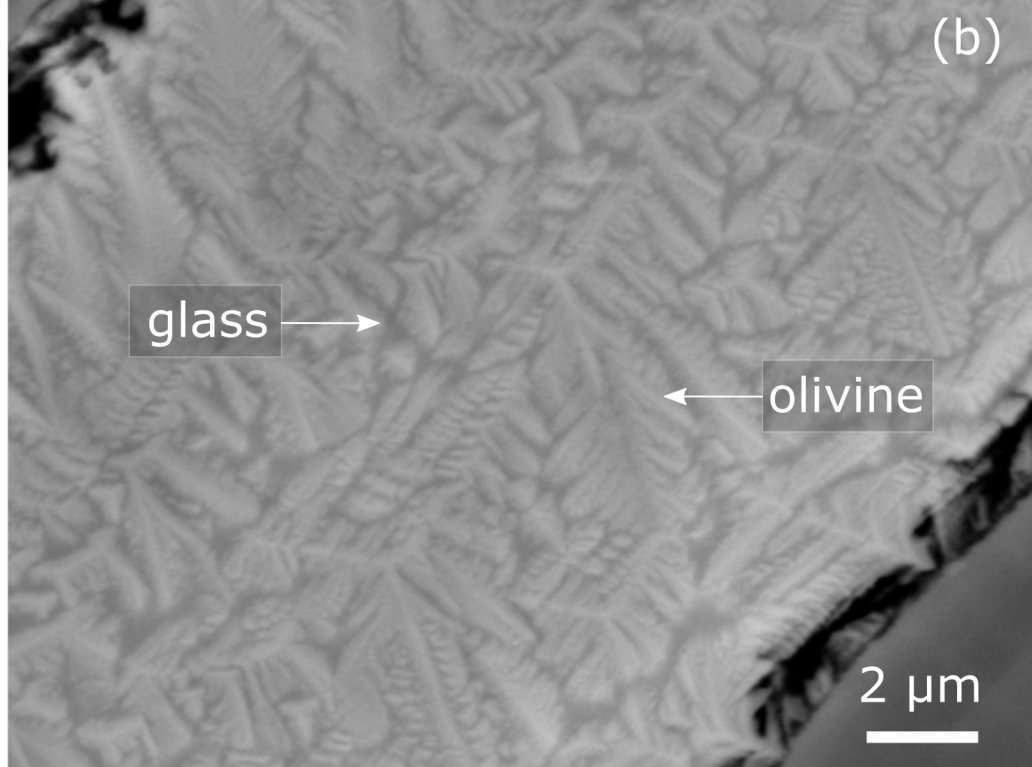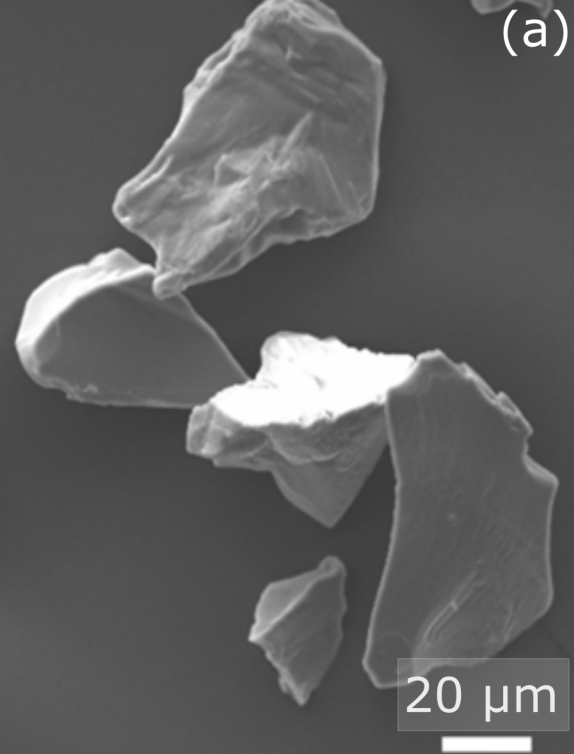| **Fo88** | molar mass | | |
|---|---|---|---|
| (Mg1.76,Fe0.24)2SiO4 | 148.21 | g/mol | |
| MgO1.76 + FeO0.24 | 88.16 | | |
| Mg(0.8)Fe0.2CO3 | 87.43 | g/mol | |
| CO2 | 44 | g/mol | 45 wt.% Fo88 |
| MgO1.76 + FeO0.24+2CO2 | 176.16 | | 79.272 |
| Olivine + 2CO2 | 236.21 | g/mol | 106.2954 |
| **Ratio max carbonation** | **74.58%** | | **74.58%** |
| | | | |
| **glass** | | | |
| (Mg1.50,Fe0.50)2SiO3 | 126.45 | g/mol | |
| MgO1.50 + FeO0.50 | 82.4 | | |
| Mg(0.75)Fe0.25CO3 | 92.125 | g/mol | 55 wt.% glass |
| CO2 | 44 | g/mol | 93.72 |
| (Mg1.50,Fe0.50)2SiO3+CO2 | 170.4 | | 117.9475 |
| GLASS + CO2 | 214.45 | g/mol | **79.46%** |
| **Ratio max carbonation** | **79.46%** | | |
| | | | |
| | | **Fo88+glass** | Average |
| | | MT composit | 172.992 |
| | | | 224.2429 |
| | | **Ratio max ca** | **77.14%** |

968

Figure 1. Powdered mine tailings observed under SEM (a) secondary electron image of powdered and cleaned sample used for the experiments. The grain surfaces are free of any adhered particles (b) angle selective back scattered image of a polished section of mine tailings showing the olivine crystals (white), embedded in glass (gray matrix) resulting a dendritic texture.

Figure 2. Mineralogical analysis of experimental run products (a) Element mapping (SEM) performed on a polished section the run product of experiment MT2 (T = 523 K and P = 30 MPa), showing formation of magnesite in large quantities (color coded by blue (Fe), green (Si) and red (Mg)). Magnesite crystals are shown in pink and initial silicate glass and traces of phyllosilicate is shown in green. A very small amount of iron oxide phases (not detectable through XRD) was observed only in this region of the sample and is marked in blue. (b) SEM secondary electron (In-lens detector) image of the same experimental run product taken on carbon coated powder showing euhedral grain of Fe-bearing magnesite (-as shown in SEM-EDX spectra) embedded in phyllosilicate. (c) X ray powder diffraction pattern of non-treated mine tailings sample and the run products of the three batch experiments, showing the progressive disappearance of olivine (O) peaks and the formation of magnesite (Mgs) during the reaction at high pressure and high temperature. The other secondary phases were phyllosilicates (Phy), and hematite (Hem). The peaks labeled (C) in the non-treated sample are the reflections of corundum which was added to the sample as the internal standard to quantify the fraction of glass (amorphous) in the initial non-reacted main tailings.
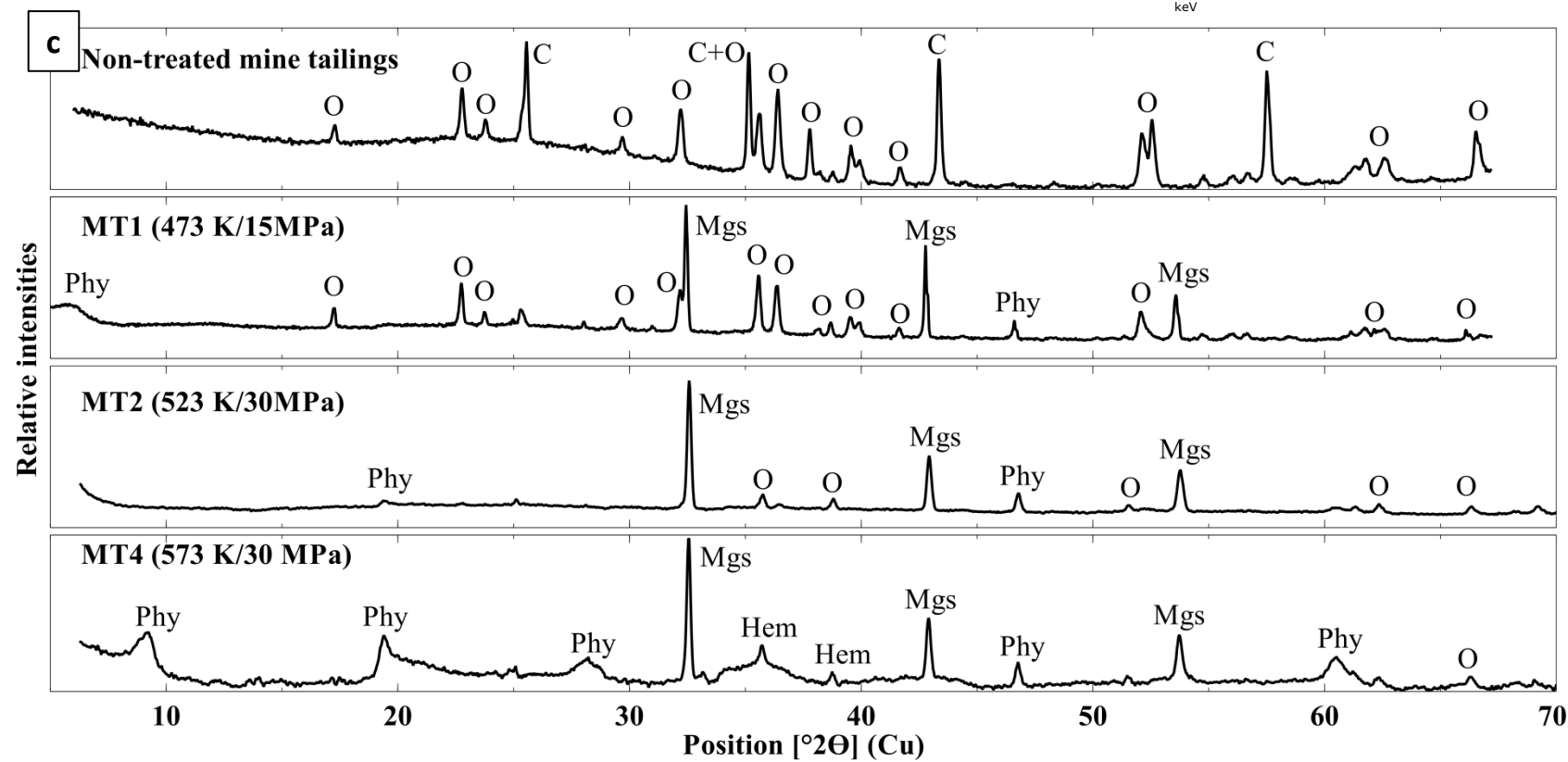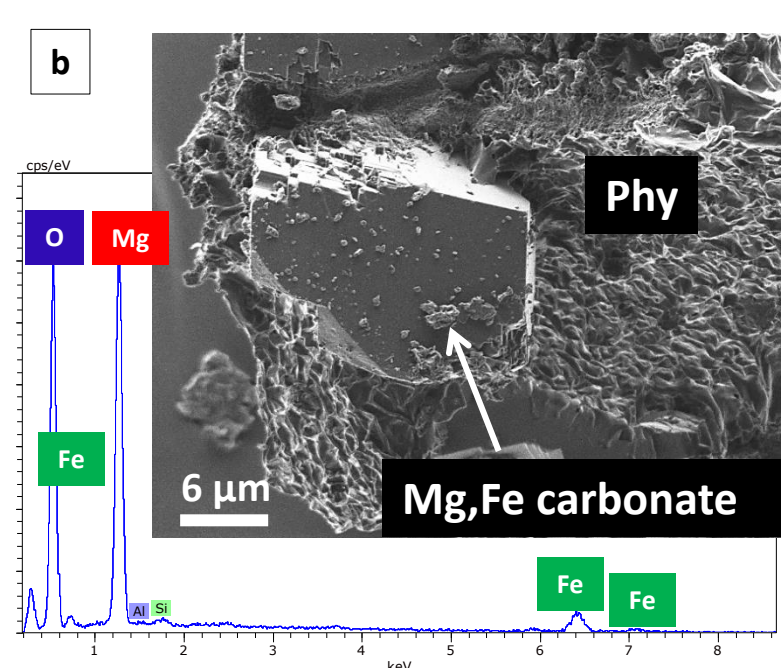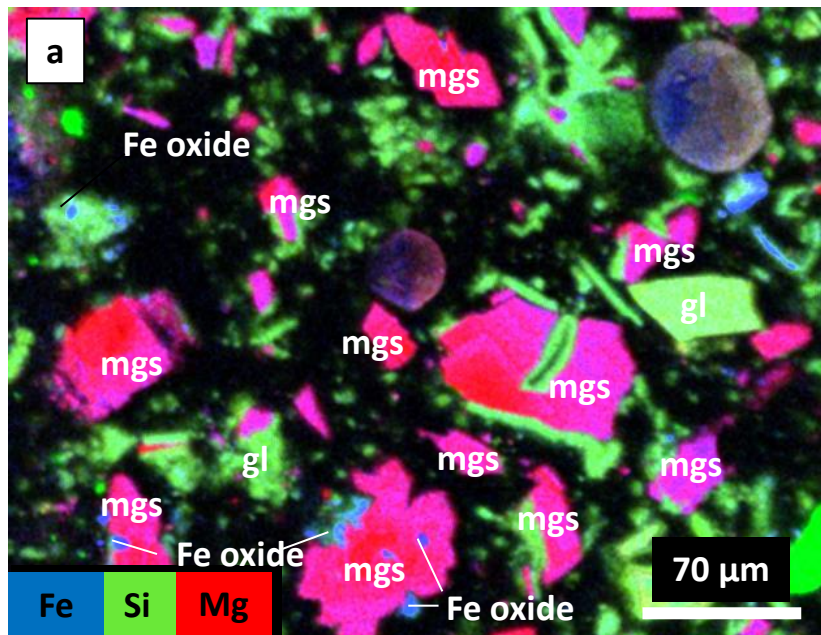
Figure 3. (a) SE image of the experimental run product at 473 K/15 MPa, showing some remaining glass, thin phyllosilicate layer formed around mine tailings and newly formed magnesite crystals; (b) a grain of mine tailing with olivine embedded in glass, which reacted to form anhedral magnesite crystals; (c) large magnesite crystals formed at 523 K/ 30 MPa showing Fe, Mg compositional zoning, and phyllosilicates which apparently detached from the original grains; (d) glass altered at 573 K/ 30 MPa forming a thick phyllosilicate layer.

Figure 4. Variations in the production of $H_2$, measured in the gas phase as a function of time (red points). The blue points represent blank experiments, which didn't yield any measurable concentrations of hydrogen. The error bars around the data points (smaller than the marker for most of them) represent a 5% uncertainty associated with the concentration measurements of hydrogen ($H_2$) by gas chromatography.
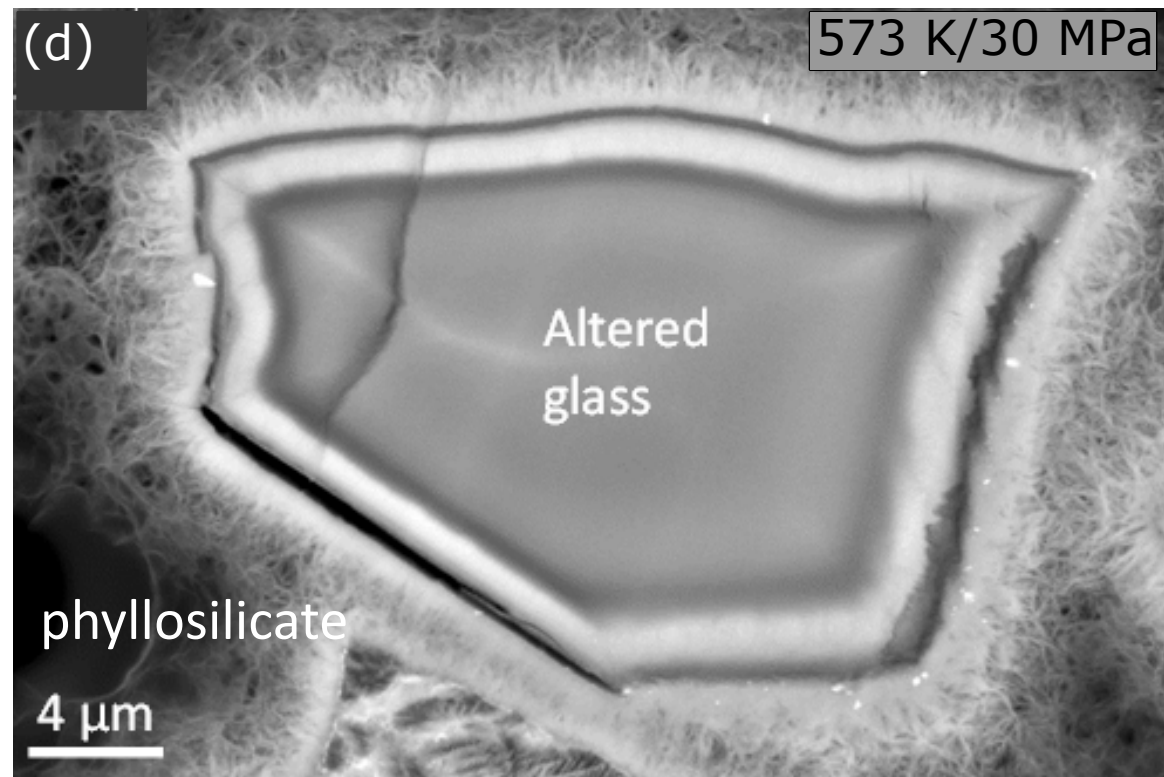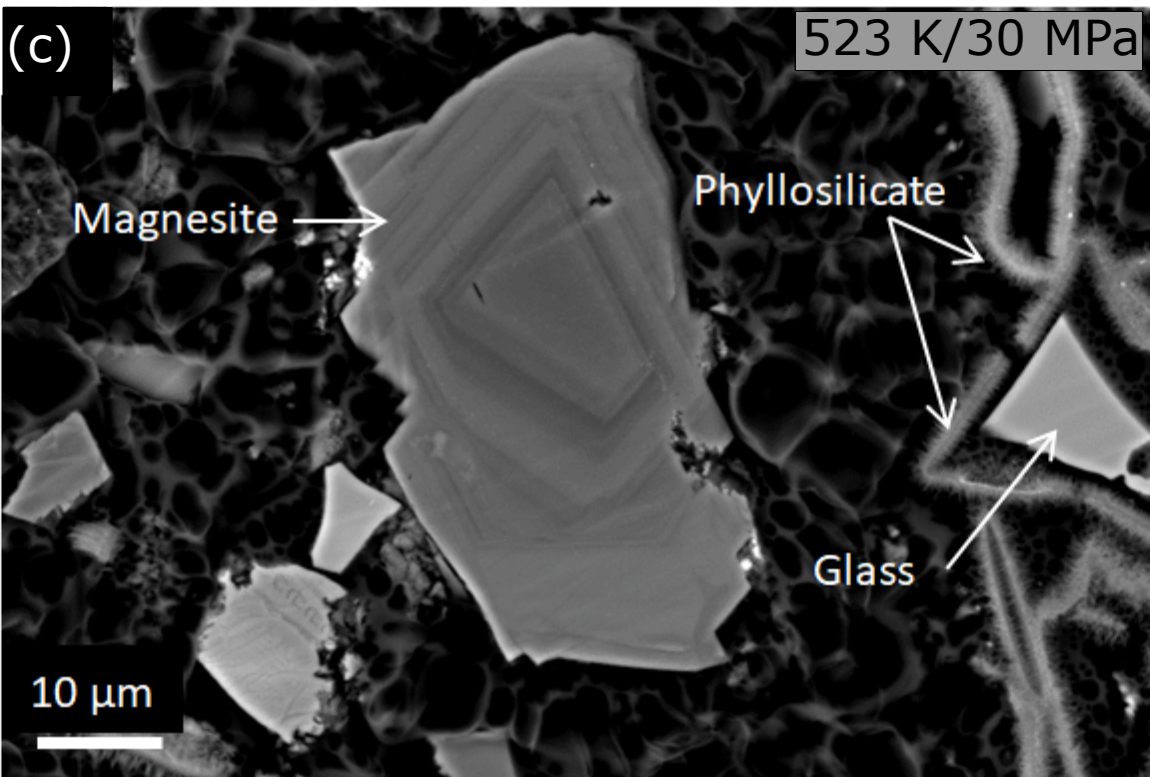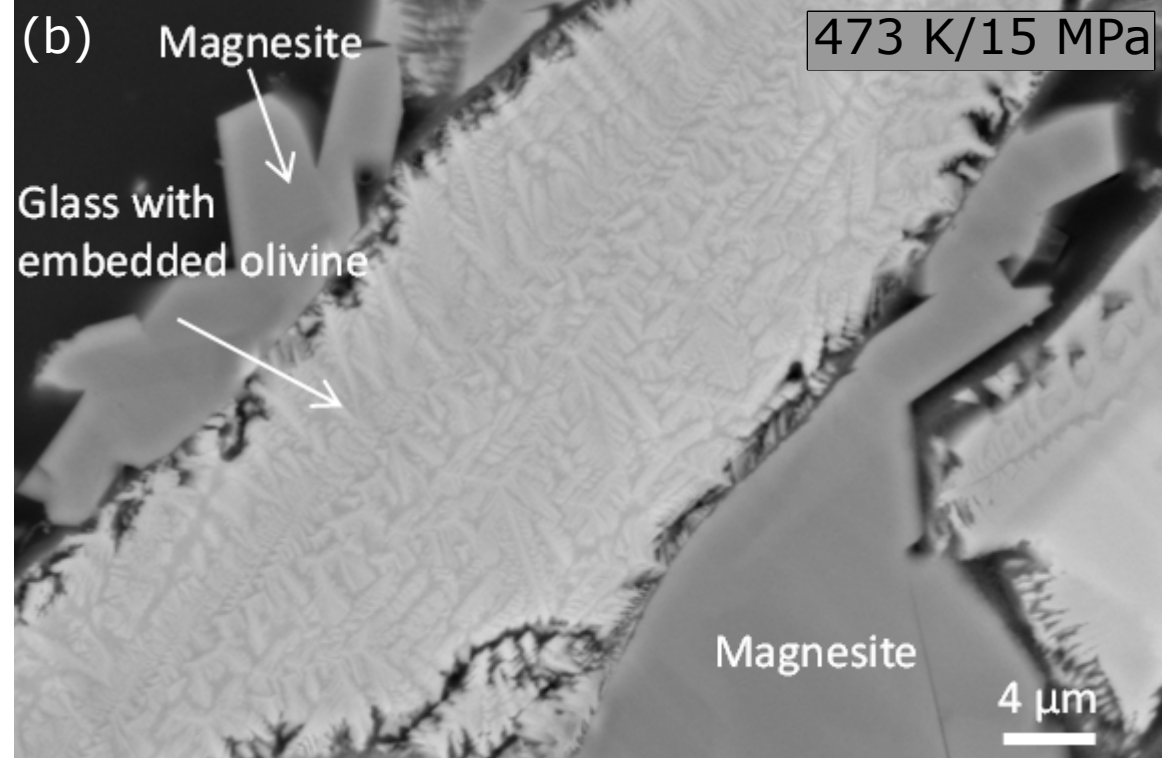
Figure 5: Quantities of magnesite precipitation and hydrogen production, obtained during the reaction of New Caledonian mine tailings, with $CO_2$-saturated water and as a function of temperature. The diagram emphasizes the competition between the two reactions. The shaded area indicates the temperature range at 30 MPa, recognized as the best conditions for the simultaneous carbonation and hydrogen production from mine tailings.

(a) (b) glass olivine

20 µm 2 µm

**a**

Fe oxide

mgs

mgs

mgs

gl

mgs

mgs

mgs

gl

mgs

mgs

mgs

mgs

Fe oxide

mgs

Fe oxide

| Fe | Si | Mg |

70 μm

**b**

cps/eV

O    Mg

Fe

Al  Si    Fe  Fe

1    2    3    4    5    6    7    8    keV

Phy

6 μm

Mg,Fe carbonate

**c**

Relative intensities

**Non-treated mine tailings**

O    C    C+O    O    C    C

O    O    O    O    O    O    O

**MT1 (473 K/15MPa)**

Phy    O    Mgs    Mgs

O    O    O    O    O    Mgs

O    O    Phy    O    O    O

**MT2 (523 K/30MPa)**

Mgs

Phy    Mgs    Mgs

O    O    Phy    O    O    O

**MT4 (573 K/30 MPa)**

Mgs

Phy    Phy    Hem    Mgs    Mgs

Phy    Hem    Phy    Phy    O

10    20    30    40    50    60    70

**Position [°2Θ] (Cu)**

(a) 473 K/15 MPa — magnesite, glass, phyllosilicate

(b) 473 K/15 MPa — Magnesite, Glass with embedded olivine, Magnesite

(c) 523 K/30 MPa — Magnesite, Phyllosilicate, Glass

(d) 573 K/30 MPa — Altered glass, phyllosilicate

(a)

T = 473 K
P = 15 MPa

(b)

T = 523 K
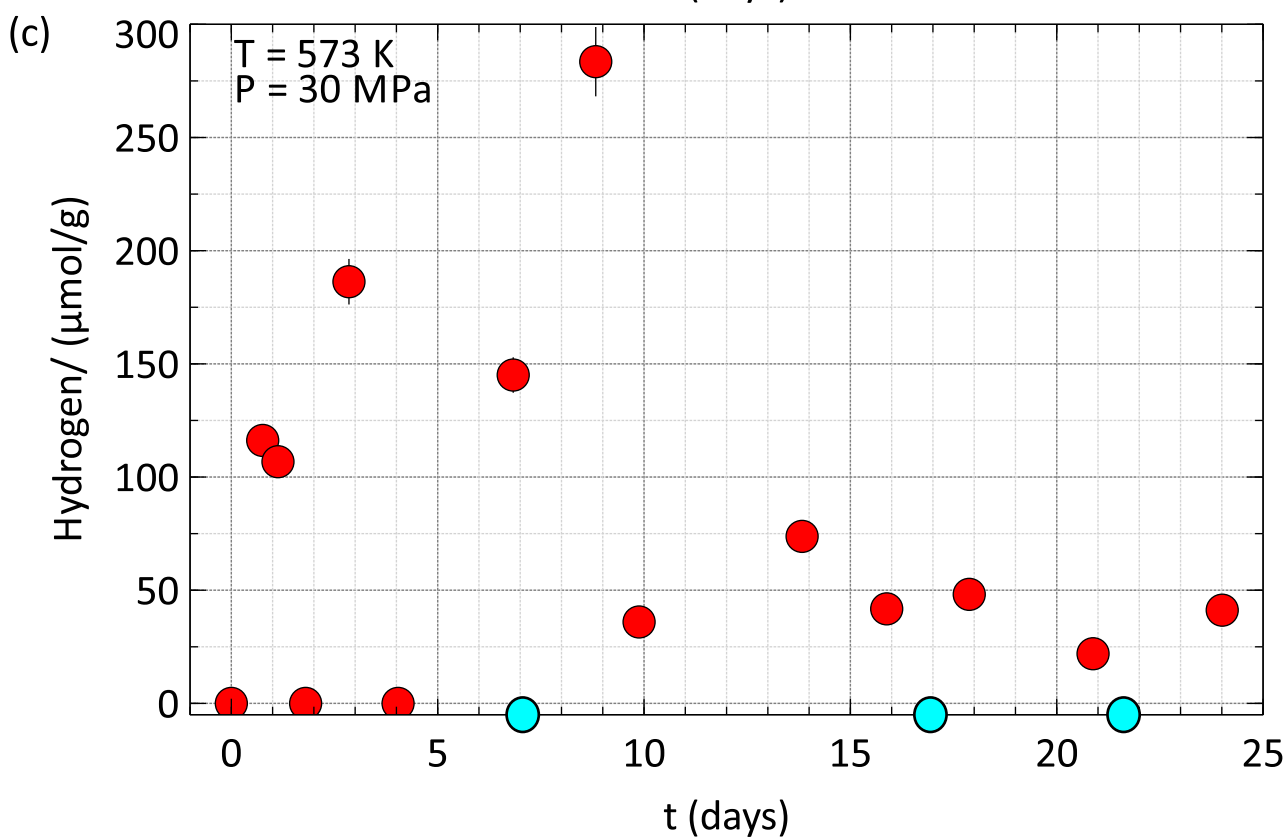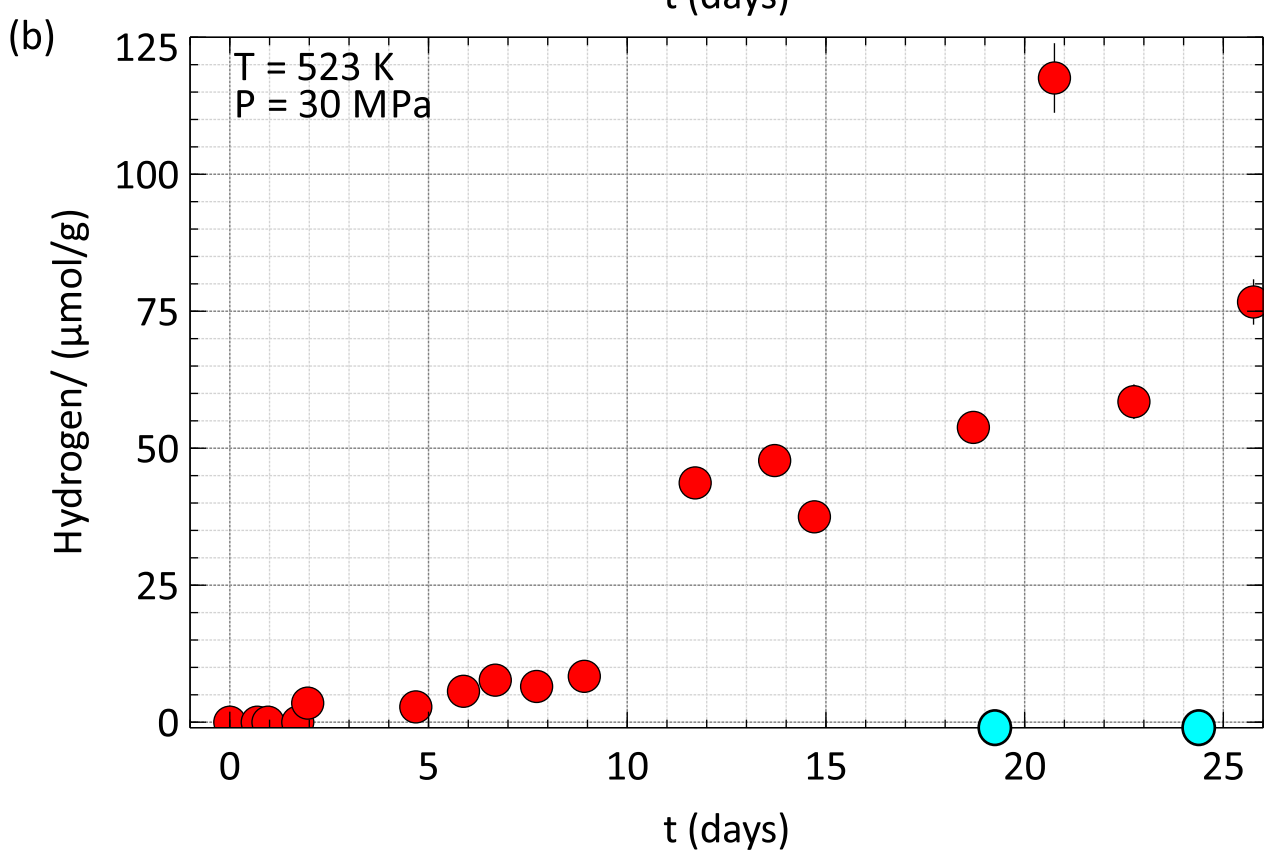P = 30 MPa
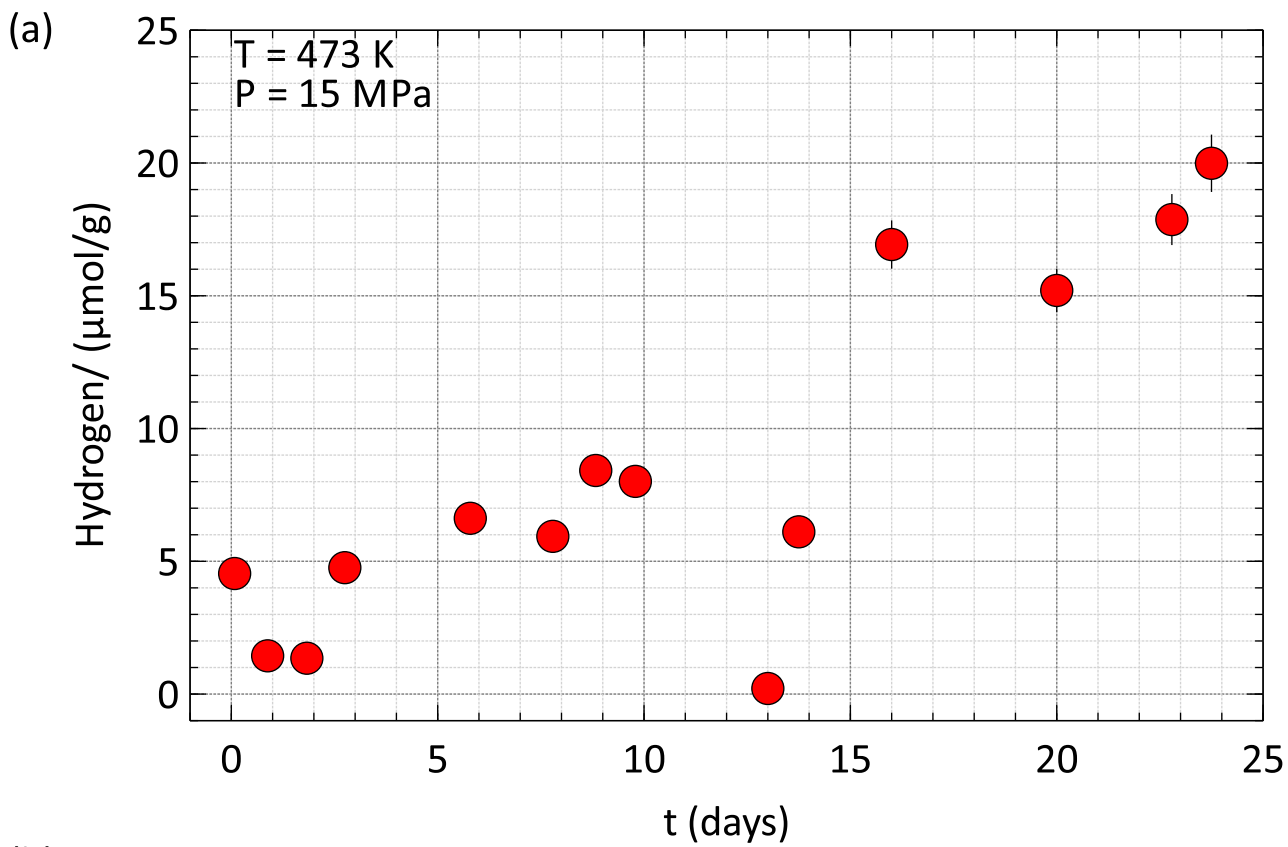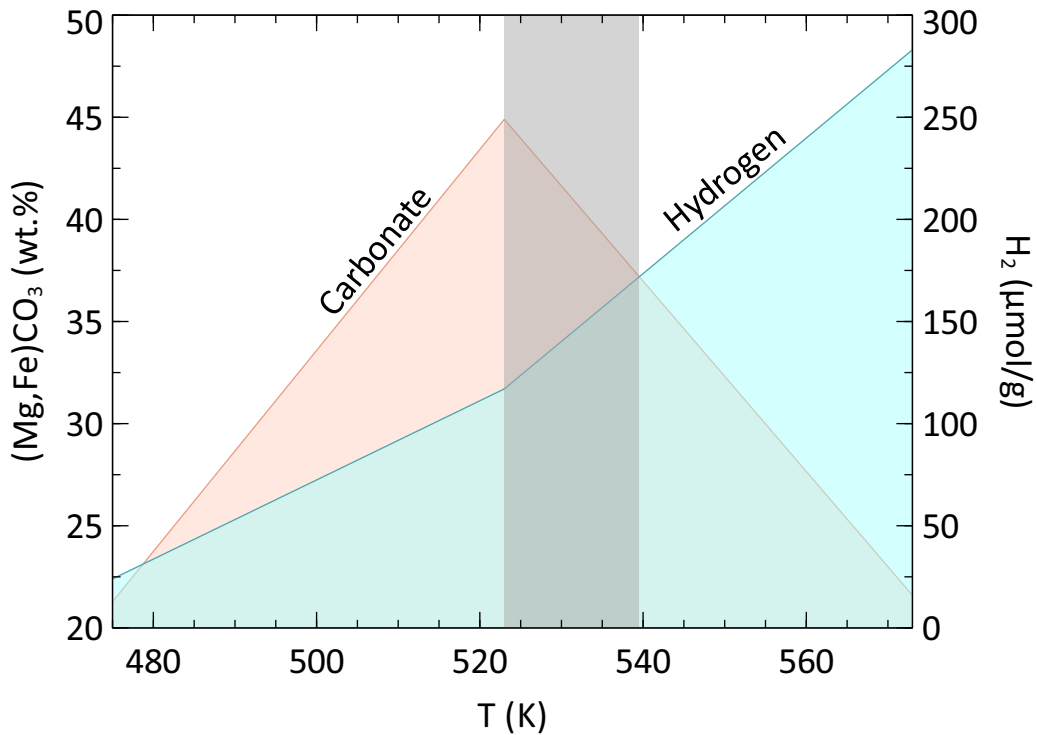
(c)

T = 573 K
P = 30 MPa

Table 1. The chemical composition of New Caledonian mine tailings, determined by electron probe micro analysis (EPMA) performed on crystalline olivine and glass, expressed in weight percent (wt.%) of corresponding oxide.

| | $Na_2O$ | MgO | $SiO_2$ | $Al_2O_3$ | $K_2O$ | CaO | $TiO_2$ | $Cr_2O_3$ | FeO | MnO | CoO | NiO | Total | Mg#[a] |
|---|---|---|---|---|---|---|---|---|---|---|---|---|---|---|
| Olivine | 0.05 | 47.27 | 40.88 | 0.07 | 0.01 | 0.11 | 0.04 | 0.02 | 11.67 | 0.12 | 0.05 | 0.38 | 100.68 | 0.88 |
| Glass | 0.04 | 23.94 | 55.22 | 3.81 | 0.01 | 0.48 | 0.06 | 1.68 | 14.23 | 0.9 | 0.01 | 0.01 | 100.39 | 0.75 |
| Avg[b] | 0.05 | 35.61 | 48.05 | 1.94 | 0.01 | 0.30 | 0.05 | 0.85 | 12.95 | 0.51 | 0.03 | 0.20 | 100.54 | 0.82 |

[a]The magnesium number; Mg#= Mg/(Mg+Fe)

[b]Average composition of mine tailings

Table 2. Summary of experimental conditions, pH of the solutions, carbonate yields, measured hydrogen and methane in each batch experiment.

| | P(total) (MPa) | P(CO$_2$)[a] (MPa) | T (K) | t (days) | Mine tailings (g) | Pure water (g) | water/rock ratio | Initial pH[c] | CO$_2$ storage[d] (g/kg) | Hydrogen(max) measured by GC (g/kg)[e] | Methane(max) (g/kg)[e] |
|---|---|---|---|---|---|---|---|---|---|---|---|
| MT1 | 15 | 13.1 | 473 | 25 | 2.0 | 201 | 100 | 3.55 | 114.4 | 0.04 | nd |
| MT2 | 30 | 26.4 | 523 | 25 | 1.7 | 170 | 100 | 3.65 | 320.5 | 0.24 | 0.02 |
| MT4 | 30 | 28.2 | 573 | 24 | 1.7 | 170 | 100 | 3.94 | 118.5 | 0.57 | 0.05 |
| MT2b (blank) | 30 | 26.4 | 523 | 24 | - | 170 | - | - | nd | nd | 0.01 |
| MT4b (blank) | 30 | 28.2 | 573 | 24 | - | 170 | - | - | nd | nd | 0.06 |

[a]Calculated for the given temperature and P(total) using the thermosolver software (Barnes and Koretsky, 2004)
[b]Solid mass to solution volume ratio
[c]pH at experimental conditions calculated using the CHESS geochemical code (van der Lee and De Windt, 2002)
[d]grams of molecular CO$_2$ trapped in 1 kg of mine tailings
[e]grams of hydrogen (H$_2$), or methane (CH$_4$) produced per 1kg of mine tailings
nd = not detected in the gas chromatography analysis

Table 3. Production of hydrogen in each experiment estimated from FeO analysis. Reaction progress calculated based on the hydrogen production is also reported (Rx%).

| Exp. | Wt (g) | T (K) | FeO wt% | FeO (mmol/g) | $\Delta$FeO (mmol/g)* | Eq. $H_2$[a] ($\mu$mol/g) | Eq. $H_2$ (g/kg) | Rx% |
|---|---|---|---|---|---|---|---|---|
| MT[b] | 2 | - | 9.39 | 1.31 | 0 | no | | |
| MT1 | 2 | 473 | 9.65[c] | 1.34 | -0.03 | -15 | -0.03 | -2.3 |
| MT2 | 2 | 523 | 7.74 | 1.08 | 0.23 | 115 | 0.23 | 17.6 |
| MT4 | 2 | 573 | 5.61 | 0.78 | 0.53 | 265 | 0.53 | 40.5 |

[a]Equivalent hydrogen

[b]MT refers to non-treated mine tailings

[c]This is an analytical error (see text), causing the successive negative values.

Table 4. Comparison of ex-situ $CO_2$ sequestration at 573K <T>423 K and P<30 MPa

| Composition | d (μm) | P (MPa) | T (K) | t (h) | Solution | $CO_2$ (g/kg)[a] | Reference |
|---|---|---|---|---|---|---|---|
| chrysotile (OK) | 425-1000 | 12.4 | 428 | 1 | 1M NaCl, 0.64M NaHCO$_3$ | 183.0 | Bobicki et al., 2015 |
| chrysotile (Pipe) | 425-1000 | 12.4 | 428 | 1 | 1M NaCl, 0.64M NaHCO$_3$ | 157.0 | Bobicki et al., 2015 |
| Olivine | 20-80 | 15 | 423 | 336 | supercritical $CO_2$ | 261.0 | Garcia et al.,2010 |
| Olivine | 40-63 | 15 | 473 | 600 | $CO_2$-saturated water | 114.4 | This study_MT1 |
| Olivine | 40-63 | 30 | 523 | 600 | $CO_2$-saturated water | 320.5 | This study_MT2 |
| Olivine | 40-63 | 30 | 573 | 576 | $CO_2$-saturated water | 118.5 | This study_MT4 |

[a]Grams of molecular $CO_2$ captured by one kg of starting material

Table 5. Comparison of hydrogen production by experiments conducted at 473 and 573 K.

| Reference | Material | Solution | pH | T | t (h) | [b](H$_2$ g/kg) |
|---|---|---|---|---|---|---|
| Malvoisin et al., 2013 | [a]CARBOF | water | 6.9 | 473 | 69.2 | 0.01 |
| Crouzet et al., 2017 | FeO | 0.05M acetic | 3 | 473 | 72 | 5.34 |
| This study | mine tailings | CO$_2$+water | 3.6 | 473 | 66 | 0.07 |
| Malvoisin et al., 2013 | CARBOF | water | 6.9 | 573 | 141 | 1.38 |
| Crouzet et al., 2017 | FeO | water | 6 | 573 | 144 | 2.18 |
| This study | mine tailings | CO$_2$+water | 3.9 | 573 | 164 | 2.26 |

[a]CARBOF=carbonated basic oxygen furnace steel slag

[b]grams of H$_2$ produced by 1 kg of FeO

Highlights

- New Caledonian mine tailings can be used for ex-situ $CO_2$ sequestration and $H_2$ production.

- Mg and Fe incorporation among the secondary phases play an important role.

- Maximum yields obtained at 523 K and 540 K at $pCO_2$=30 MPa.

- A novel method of valorization of Fe, Mg containing mine tailings.

- Cost effective method to treat $CO_2$ emissions and energy demands.